Response to anonymous reviewer comments

Dear Reviewers,

We would like to thank you both for your thorough reviews of our manuscript. We feel that your comments prompted insightful discussion that has greatly improved our manuscript. Below we include our responses to your comments in blue. We have also made adjustments to the manuscript where necessary and have included our revised manuscript with tracked changes.

Many thanks,

Courtney Quinn, Terence O'Kane, and Vassili Kitsios

REVIEW 1

General comments

This manuscript is exploring the use of covariant Lyapunov vectors (CLVs) to build the error covariance matrix in ensemble Kalman filtring methods. The set of vectors is selected based on the computation of a local Kaplan-Yorke dimension based on the finite time Lyapunov exponents. This approach is implemented in the context of a multi-scale system mimicking the (coupled) dynamics of a coupled tropical ocean-atmosphere system and the extra-tropical atmosphere. Different strategies of observation are then evaluated. It is found that observation within the atmosphere is essential,and that the variable number of CLVs to be used in building the error covariance matrix is a successful strategy for strongly coupled data assimilation. Very interesting results are also obtained with the observation sampling of a shadowing trajectory, leading to measurement correlations.

This is an interesting manuscript exploring many aspects of the strongly coupled data assimilation and I would in principle recommend publication of this work.

We thank the reviewer for the positive evaluation.

I have however an important concern on the use of the local Kaplan Yorke dimension and the CLVs that should be addressed before publication. It seems to me that the use of both is inconsistent. Let me clarify my point. When computing the FTLEs, one can use either the QR (associated with the backward Lyapunov vectors) decomposition,the Forward Lyapunov vectors obtained with backward integration in time, or the local amplification along the CLVs.

Although all these are giving the appropriate asymptotic Lyapunov exponents, they are not providing similar variability of these quantities as illustrated for instance in Vannitsem and Lucarini (2016) you quoted. So if you use the QR decomposition and then select the CLVs on that basis this is probably not optimal.

We have considered the reviewer's concern and are in agreement that the use of the two quantities could produce inconsistencies. To clarify, we use the QR decomposition method to calculate the FTLEs, which would give amplification rates for the backward Lyapunov vectors rather than the CLVs. However, in this case we argue that the way in which we utilise the FTLEs does not create an inconsistency with the CLVs in that we are not assigning any particular FTLE to a CLV. Rather, the backward FTLEs are used only to produce an adequate estimate of the number of CLVs to retain in constructing the covariance matrix. The true local dimension of the system may be different from the quantity computed, but the Kaplan-Yorke dimension calculated from the backward FTLEs still produces a sufficient upper bound. We expand on this point further below.

Figure 1 shows the finite-time Kaplan-Yorke dimension of a segment of the example model run from Sections 2 and 3 in the manuscript (compare to Figure 5 in manuscript). The top panel is the dimension measure, while the bottom is the ceiling of the dimension measure which is used to select the number of CLVs for constructing the covariance matrix. We compare the two different methods for calculating the CLVs that the reviewer mentions: growth rate along CLVs (FTCLEs) and QR decomposition (FTBLEs). We observe that for our particular nonlinear system, the QR decomposition method consistently gives a larger estimate for the Kaplan-Yorke measure than the amplification along CLVs, and therefore implies retaining more CLVs in the analysis. We maintain that a higher number of retained CLVs will not harm the DA, while too few CLVs potentially could. Specifically, where the positive CLVs are closely aligned, the DA requires the inclusion of most of the additional neutral and stable CLVs to avoid ensemble collapse (further discussion of this point on the following page). Thus, Kaplan-Yorke is an effective choice to determine the rank of the background covariance matrix despite the any inaccuracies due to degeneracy in the unstable directions. Additionally, we mention that in order to obtain the growth rate of the CLVs, one needs the accurate forward model. Since we are calculating the CLVs from the ensemble mean trajectory within the DA experiments, we do not have an accurate future trajectory and therefore no forward model (due to the state dependence of the Jacobian). For these reasons we maintain that the FTLEs from the QR method are a sufficient for our analysis at hand.

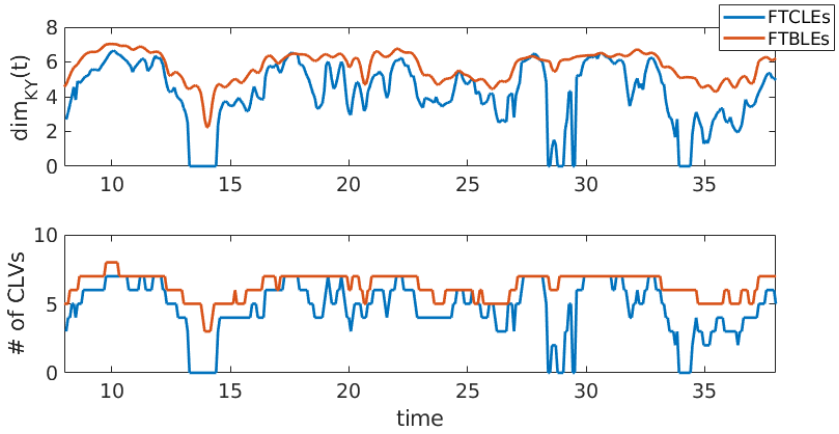

Figure 1: Comparison of finite-time Kaplan-Yorke dimension calculated using the growth rates of CLVs (FTCLEs) and the QR method (FTBLEs).

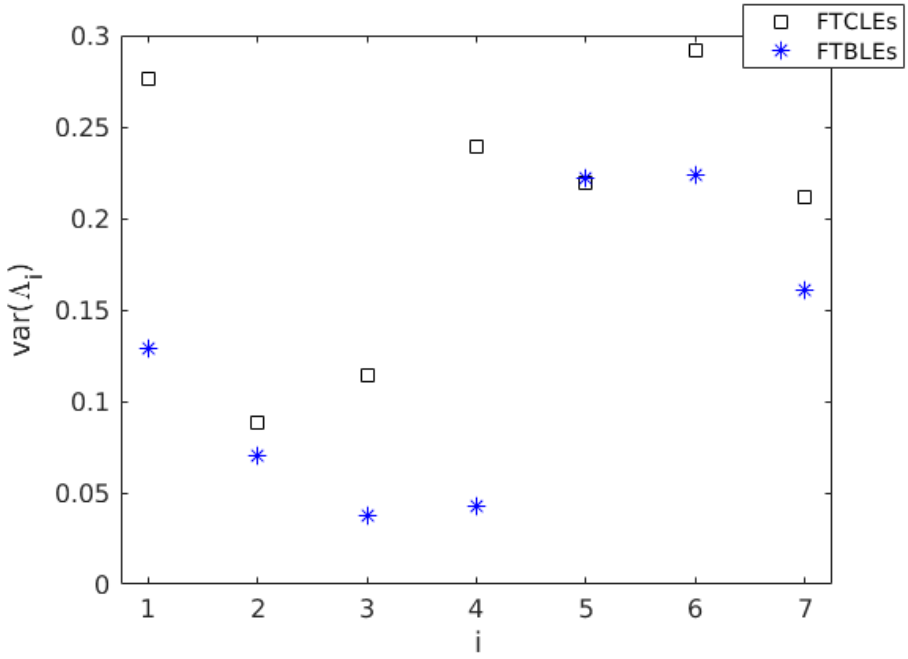

Figure 2: Comparison of variance of the individual FTLEs calculated using the growth rates of CLVs (FTCLEs) and the QR method (FTBLEs).

Alternatively, if you use an estimate of the FTLE using the amplification along the CLVs then the "dimension" of the subspace of instabilities is not the same and one can wonder what is the signification of this quantity. This is related to your comment at line 14 of page 8 indicating that higher dimension is associated with more important alignment of CLVs. Imagine for instance that several CLVs are pointing in almost the same direction with large amplifications, then the dimension would be large but intuitively (as they point all in the same direction) we would expect a low dimension. The specific way you compute the FTLEs and the local dimension should therefore be clarified, and probably I would not call it "dimension". Furthermore, if the KY dimension is computed with the local amplification rates of the backward Lyapunov exponents, a comparison should be made with the use of the backward Lyapunov vectors in building the error covariance matrix. It would have been my first choice in view of the fact this is much less costly than the CLVs.

The reviewer is correct in that the finite-time Kaplan-Yorke measure is not necessarily the true local dimension. However, this measure is giving an indication of local dimension combined with alignment. We explain this through an examination of two difference time steps in the benchmark DA experiment (Section 5.2 in the manuscript) where a high Kaplan-Yorke measure is recorded and the FTLE behaviour is similar. The alignment of the CLVs and the FTLEs (computed using the QR decomposition method) are shown in Figure 3. In both cases we see that there are 2 equally strong leading unstable FTLEs, 3 positive but near zero FTLEs, and one weakly stable FTLE. In the first column ($t = 306.24$) we see that the 5 leading CLVs are strongly aligned as well as the two most stable (8 and 9). The dimension based on alignment would then intuitively be around 4, and one would need to select the set of CLVs that are not aligned. In our method since $\dim_{KY} > 7$ we would retain 8 CLVs, therefore accounting for the strong alignment of the leading CLVs and retaining all necessary directions. In the second column ($t = 705.04$) the case is quite different in that the leading CLVs are not strongly aligned, but there is strong alignment of CLVs 4-6 and pairs 3,7 and 8,9. This would give an alignment-based dimension around 5, but again we need to retain up to the 8th CLV to span the local manifold. While one could create a method based on alignment for selecting directions, we point out that the actual criteria for "strong alignment" is arbitrary and one could risk excluding a significant direction.

With regards to using the backwards Lyapunov vectors (BLVs), if one is using the QR method then the backwards Lyapunov vectors computed are orthogonal by construction. We therefore do not see the same behaviour of alignment of the vectors. We ran the benchmark DA experiment (Section 5.2 in the manuscript) using a variable number of BLVs based on the Kaplan-Yorke measure computed using the QR decomposition method (statistics shown in Table 2 of revised manuscript). We see that the variable BLVs and variable CLVs perform comparably. While all experiments could be run with the BLVs as suggested by the reviewer, we aim to show the functionality of using the CLVs as they provide additional information about the phase-space dynamics which can

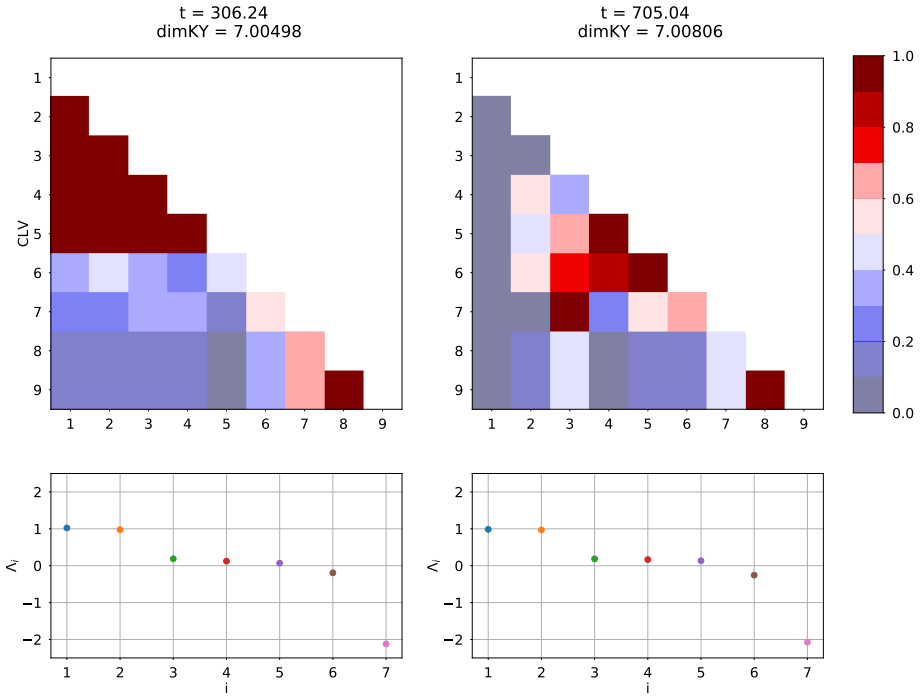

Figure 3: We compare the alignment of the CLVs at two time steps of the benchmark DA experiment (section 5.2 in the manuscript). The two time steps have similar Kaplan-Yorke measure and distribution of leading FTBLEs, shown in the bottom panels. We observe that the behaviour of the alignment can be vastly different for similar FTBLE behaviour, however the method of retaining CLVs based on the Kaplan-Yorke measure gives a reliable way to reflect the true local dimension regardless of alignment.

be analysed *a posteriori*.

We have made the following additions to the manuscript to address all the above concerns and clarify our methods:

- We have added a paragraph and figure to Section 3 of the manuscript to discuss the differences in calculating the FTLEs.
- We have added Figure 3 along with a discussion of alignment, dimension, and relevance to ensemble DA in Section 4.2.
- We have added the statistics for using BLVs with variable Kaplan-Yorke measure in the benchmark DA case of Section 5.2.

Specific comments:

1. Figure 3, you mentioned 2 neutral Lyapunov exponents. I am wondering why you have two such exponents. Is there any specific symmetries allowing for that? Isn't it a numerical artifact?

   For clarification, the model has a neutral and a near-neutral Lyapunov exponent. The near-neutral exponent comes from the weak coupling to the extratropical subsystem ($c_e = 0.08$). If one were to set $c_e = 0$, the extratropical subsystem would be completely uncoupled from the tropical and ocean subsystems, and it would retain its symmetry $[x_e, y_e, z_e] = [-x_e, -y_e, z_e]$. This implies an additional neutral Lyapunov exponent. However, we retain that the near-neutral exponent is important to consider within the neutral subspace in this study as the timescales of the neutral and near-neutral exponents are indistinguishable and changes in both can significantly affect the local Kaplan-Yorke measure. To improve and assess numerical precision, we have computed the Lyapunov exponents over a longer window (500,000 time steps) and show the results for the original parameter values as well as different combinations of coupling strengths set to zero in Table 1.

	λ_1	λ_2	λ_3	λ_4	λ_5	λ_6	λ_7	λ_8	λ_9
as in manuscript	0.9043	0.3052	0.0007	-0.0032	-0.4829	-0.8008	-1.8149	-12.2359	-14.5726
$c_e = 0$	0.9083	0.3029	0.0001	-0.0006	-0.4814	-0.7962	-1.8172	-12.2415	-14.5744
$c = 0$	0.9042	0.3491	0.0597	-0.0002	-0.0151	-0.3186	-1.6222	-13.4793	-14.5777
$c_z = 0$	0.9081	-0.0004	-0.0723	-0.0728	-0.1283	-0.1289	-1.1599	-13.4702	-14.5753
$c = c_z = 0$	0.9069	0.8886	0.0902	0.0001	-0.0004	-0.0741	-1.4569	-14.4801	-14.5743
$c_e = c = 0$	0.9083	0.3581	0.0692	-0.0006	-0.0007	-0.3227	-1.6360	-13.5012	-14.5744
$c_e = c = c_z = 0$	0.9083	0.9083	0.0902	0.0001	-0.0006	-0.0006	-1.4569	-14.5744	-14.5744

Table 1: Asymptotic Lyapunov exponents of coupled Lorenz model for different coupling coefficients set to 0. Lyapunov exponents computed over 5000 time units using a QR decomposition method, time step of 0.01, and orthogonalization step of 0.25.

2. Table 2. The RMSE for the extratropics are very close to each other whatever the experiments. Are the differences significant?

   We preface this response with pointing out that the statistics of Table 2 have slightly changed on fixing a numerical error in the code (see revised manuscript). In order to discuss significance of differences in the average RMSE we have to compute error bounds on the means. To do this, we perform a bootstrapping of the time series of extratropical RMSE for each of the five experiments listed in Table 2 of the revised manuscript. We resample the data (with replacement) 10,000 times and then compute

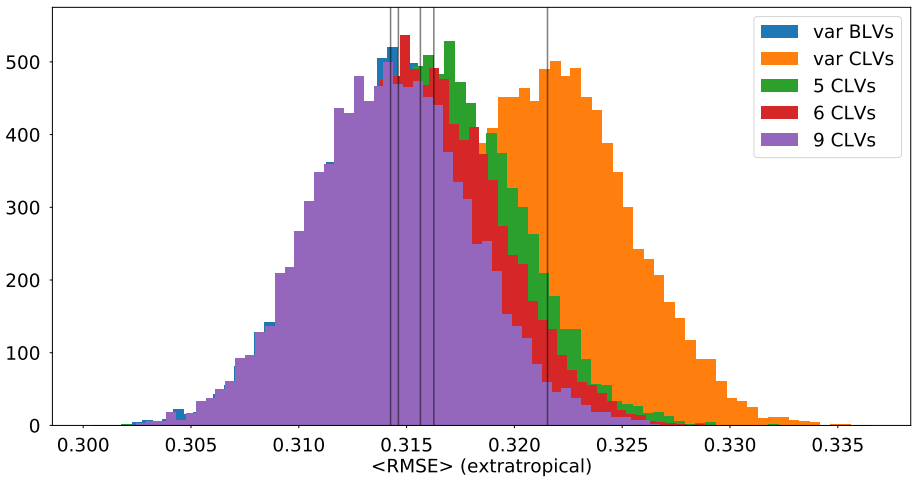

Figure 4: Histograms for the means of the resampled time-dependent extratropical RMSEs for each respective experiment. The black lines show the means of the histograms, which are approximately the values of extratropical average RMSE in Table 2 of the manuscript.

the average RMSE for each resample. This produces a distribution of average RMSE for each experiment, shown in Figure 4. Each distribution has standard deviation $\sigma \approx 0.004$, and we see that the mean of the distributions shift by less than σ between experiments with the exception of the variable CLVs experiment. The mean of the variable CLVs experiment still lies within 2σ of all the experiment distributions. In this sense we can conclude that the values listed in Table 2 of the revised manuscript are not significantly different. Additionally, we note that in the sense of quantifying the DA performance, all five methods constrain the extratropical system to a similar degree.

3. Also in Table 2. An average dimension is computed. This average is based on the QR decomposition or some estimate with the CLVs? This is related to my main point. Please clarify how it is computed.

   The average dimension comes from the FTLEs which are calculated using the QR decomposition. We have clarified this in the manuscript.

4. FTLEs are computed for 4 time units. What is happening to your analysis when this window is changed? And why choosing this specific window?

   The window of 4 time units was chosen in order to capture dimension changes related to the ENSO-like excursions in the ocean subsystem (occurring anywhere between approximately 6.5 and 27 time units). The window should therefore be long enough to filter out the intrinsic oscilla-

tory behaviour of the ocean subsystem but short enough to capture the transition to the excursion state. The period of intrinsic variability is approximately 3 time units, therefore any window between 3 and 6.5 time units should perform comparably. Decreasing and increasing the window leads to higher and lower temporal variability of the FTLEs, respectively.

5. At page 12, in the two first paragraphs of Section 5, you present how the experiment is done. As far as I understood, the CLVs are computed during a limited period of time during the assimilation period. Am I right? At first reading it was not very clear to me and it would be nice to improve the presentation of that part. In particular, a sketch of the whole process in a figure would be really useful.

   We have clarified the paragraph where we explain the computation of the CLVs within the DA framework.

6. In the partially observed CDA, you also compute a local dimension. I am wondering how the CLVs are computed there since the trajectory of the model is probably very far from reality. Moreover, it was not clear to me whether you are using the CLVs of the reality or of the model integration. Would you please clarify how you do this? It can maybe be incorporated in the general description of the experiments mentioned at point 5 above.

   The CLVs are calculated from the ensemble mean trajectory. In the cases where the full system is constrained (atmosphere-only observations), the ensemble mean remains close enough to the truth such that the CLVs can still be calculated to a sufficient accuracy. On the other hand, this is not the case when some of the subsystems are unconstrained (i.e. ENSO and extratropical-only observations). In such cases we cannot use the variable dimension method, and instead we use all 9 computed CLVs. This is valid since the forecast error covariance matrix has rank 9 in this set-up and we are projecting onto a basis of equivalent rank, regardless of the accuracy of the computed CLVs. The local dimension we are calculating comes from the QR decomposition as mentioned in the response to the main comment. While the CLVs (or BLVs) may be quite inaccurate at a given point in time, the average dimension can give an idea of variance in the unobserved subsystems. In cases where an unobserved subsystem is unconstrained, it is common to observe variance collapse in the ensemble mean of that subsystem and we subsequently record a lower average local dimension. We therefore explore methods to maintain the variance in the unobserved subsystems (i.e. increase the average local dimension), with the caveat that the instantaneous dimension will not necessarily be reflective of the true dynamics of the system. We have provided additional clarification in the manuscript about the calculation of the dynamical properties within the DA experiments.

Minor points:

1. Line 7, page 11. Please modify the notation on the brackets. It looks like a vertical rectangle.

   We have changed the text to read "... and the **subscript** $*, n$ denotes taking ...".

2. Line 20, page 11. I suppose that λ should be larger than 1.

   We have added a condition to Equation 19 specifying $\lambda > 1$.

3. Line 22, page 11. Please do not use the terminology "model error". It is confusing as model error is used when there is structural uncertainty in the model.

   We have removed the term "model" as we agree that the usage is confusing in this instance.

REVIEW 2

Main points:

1. Although the bibliography is rather dense (and better done than usual), there are still a few (very) relevant references such as Palatella and Trevisan (2015) [8]; Grudzien et al. (2018a,b) [3, 4] that are missing.

   We thank the reviewer for pointing out the additional relevant references and we will include them in accordance with the specific suggestions below.

2. Even though the number of CLVs incorporated in the DA algorithm depends on time, you still need to compute a number of CLVs corresponding to the maximum local KY, do you? So that the gain is computationally limited. If I am wrong, please explain.

   In the way that we have implemented the variable dimension, one could compute the local KY measure first and then only compute the number of CLVs corresponding to that given value at each assimilation time step. (This is due to the fact that we compute dimension with the QR-factorization approach and the CLVs with a separate algorithm - clarification of this and further discussion has been added to the modified manuscript.) With respect to computational gain, there will be an additional cost associated with computing the unstable manifold regardless of

the method. Whether or not this is realizable in high dimensional systems, or how the overall cost compares to increasing ensemble size in order to fully sample the variance are not questions we attempt to answer in this study. We rather focused on the applicability of assimilation in a variable unstable subspace for different situations of strongly coupled data assimilation (*i.e.* different types of observational subsets). We discuss the reviewer's comments regarding computational cost more within the specific points below.

3. In at least a few experiments, you need to use optimally tuned inflation (section 5.3 for instance), since it is already known that the lack of span of the unstable modes can be compensated with by a stronger multiplicative inflation. Otherwise several of your claims are undermined.

   We first preface our response with bringing to the reviewer's attention that there was a small error in the calculation of the CLVs for the results shown in the manuscript submission. We have since corrected this error and updated all of our experiments. The updated tables are included in the revised manuscript. Due to these corrected results, we now can conclude for the benchmark and atmosphere observations that all experiments are successful. The emphasis of the discussion is now regarding the variable CLV full RMSE being closest to the full rank experiments for each of the observation sets. These conclusions hold for a range of inflation values. We show in Table 2 below the results for the benchmark observations using full rank, 5 CLVs, and variable CLVs with inflation values of 1% (as in manuscript - revised values), 2%, 5% and 10%. As the lowest RMSEs occur for the 1% inflation cases, we conclude this is the optimal inflation value and leave these results in the manuscript. We have added a statement noting this to the beginning of the results section (Section 5 in the manuscript). The optimization was already done for the shadowed observations (Section 5.5), and the optimal inflation values are given in the table. All other experiments have an optimal inflation of 1%.

4. The new inflation scheme is not justified enough. Beware that it has been tested in a very specific case and does not warrant generality.

   We agree with the reviewer that our language when discussing the utility of the adaptive scaling for the Kalman gain is too strong. We have changed the language to emphasize that the adaptive scaling works in this particular case, but needs to be tested on more models to form a a more general applicability. We also have added additional justification for the proposed scheme and relate it to the work of Miller *et al* [6]. More detailed discussion of our justification can be found in response to the specific points of the following section.

5. Because of the above points, there are too strong statements in the conclusion regarding the novelty and performance of the proposed method.

Method	Observations [error variance]	⟨RMSE⟩ extratropical	⟨RMSE⟩ tropical	⟨RMSE⟩ ocean	⟨RMSE⟩ full	$\langle \dim_{KY} \rangle$
CLVs - 9 1% inflation	y_e, y_t, Y [1, 1, 25]	0.3142	0.1598	0.4948	0.4027	5.8928
CLVs - 5 1% inflation	y_e, y_t, Y [1, 1, 25]	0.3123	0.1843	0.5920	0.4550	5.8870
CLVs - variable 1% inflation	y_e, y_t, Y [1, 1, 25]	0.3215	0.1688	0.5346	0.4272	5.8863
CLVs - 9 2% inflation	y_e, y_t, Y [1, 1, 25]	0.3286	0.1893	0.5985	0.4625	5.8881
CLVs - 5 2% inflation	y_e, y_t, Y [1, 1, 25]	0.3274	0.1950	0.6083	0.4681	5.8871
CLVs - variable 2% inflation	y_e, y_t, Y [1, 1, 25]	0.3219	0.1916	0.5966	0.4594	5.8915
CLVs - 9 5% inflation	y_e, y_t, Y [1, 1, 25]	0.3564	0.2627	0.8858	0.6237	5.8832
CLVs - 5 5% inflation	y_e, y_t, Y [1, 1, 25]	0.3600	0.2665	0.8880	0.6264	5.8836
CLVs - variable 5% inflation	y_e, y_t, Y [1, 1, 25]	0.3552	0.2647	0.8747	0.6180	5.8848
CLVs - 9 10% inflation	y_e, y_t, Y [1, 1, 25]	0.4117	0.3719	1.3278	0.8799	5.8763
CLVs - 5 10% inflation	y_e, y_t, Y [1, 1, 25]	0.4187	0.3873	1.3168	0.8787	5.8824
CLVs - variable 10% inflation	y_e, y_t, Y [1, 1, 25]	0.4123	0.3731	1.3153	0.8736	5.8775

Table 2: Summary metrics of DA experiments using right-transform matrix (ETKF) and benchmark observations (y_e, y_t, Y). The angle brackets $\langle \cdot \rangle$ denote average over analysis steps. Compare to results in [11]. Parameters: analysis window 0.08, 10 ensemble members.

Again, we agree with the reviewer that too strong of language is used in regards to some of the conclusions. We note that due to our corrected results we have already adjusted some of our conclusions accordingly. We will additionally adjust the specific statements mentioned in the following section.

Specific suggestions:

1. p.1, l.5: "to determine" is a bit ambiguous as it could also need "to infer" which would be a bold statement. I guess you meant "to prescribe", right?

We have changed the statement to read "to prescribe" instead, as this was our intended connotation.

2. p.2, l.2: "implying very large ensemble sizes are needed" → "implying that very large ensemble sizes are needed

   We have amended the sentence.

3. p.3, l.6: What are "local CLVs"? I know local LEs, but not local CLVs.

   This was a typo. We were referring to the CLVs calculated at a given time. We have removed the term "local".

4. p.3: Even though the beginning of the paper is very good and enjoyable, reading "We also examine the role of correlated versus random observational errors.", "along with a novel scheme for adaptive Kalman gain inflation." at the end of the introduction is odd as these two subjects do not seem directly connected to the main objective of the paper, and they seem, at this stage of the reading, unnecessary.

   We can agree that the statements are superfluous. We will save the discussion of these two topics for when they arise in the study.

5. p.4, l.18: "uncentering parameters": please explain what this means.

   The terminology "uncentering" was originally used in the Peña and Kalnay study [9] and refers to the uncentering of the unstable zero equilibrium in the classical Lorenz model. Dynamically, the k_1 and k_2 values used in the manuscript allow for the second unstable asymptotic Lyapunov exponent (for $k_1 = k_2 = 0$: $\lambda_1 = 0.91, \lambda_2 = 0, \lambda_i < 0$ for $i > 2$).

6. p.4, l.27: "We are interested in analysing both the local and global dynamics of system (1).": I guess you mean the short-term and asymptotics dynamics - your words lack accuracy here.

   That is precisely what we meant. We will change the language as suggested.

7. p.6, l.16: Can you be sure/prove that the last digits of 5.9473 are relevant?

   We do not claim that the last digits are relevant, they are included only as the Lyapunov exponents were given up to four digits.

8. p.7, l.2: "approach their corresponding asymptotic values" → "approach their corresponding LEs asymptotic values"

   We have changed the sentence to read "approach the asymptotic Lyapunov exponent values".

9. p.7, l.3: You have to discuss/justify more the concept of local KY dimension. This is the main idea of your paper.

   We have added some additional discussion around the concept of local dimension used in our manuscript as suggested.

10. p.7, l.4: "We see the local dimension" → "We see that the local dimension"

    We have amended the sentence.

11. p.7, l.13: "the cocycle of": Please explain what a cocycle is. How is it connected to (1)?

    In relation to system (1) in the manuscript, a cocycle is the forward and backward mapping of solutions under the tangent dynamics. The cocycle is then given as $\mathcal{A}(x(t), \tau) = \mathrm{e}^{\tau Jf(x(t))}$ where Jf denotes the Jacobian of f, the right-hand-side of system (1). We have clarified this in the manuscript and have restructured the sentence such that *a prior* knowledge of the term cocycle is not assumed.

12. p.8, l.7: "local time-varying Kaplan-Yorke dimension.": what is its interpretation? This is key to your paper.

    We have added a more descriptive explanation of the local Kaplan-Yorke dimension here, particularly relating to our implementation and its relation to the CLV behaviour.

13. p.8, l.16-19: Palatella and Trevisan (2015) [8] could be mentioned here.

    We have added the reference.

14. p.9, l.4: "Suppose there exists" → "Suppose that there exists"

    We have amended the sentence.

15. p.9, Fig.5, legend: replace the "v" symbol by "or" for the sake of clarity.

    We have changed the legend accordingly.

16. p.9, l.9-11: The errors are also supposed uncorrelated in time (white).

    We have clarified the assumption of temporally uncorrelated errors in the description of the Kalman filter method.

17. p.9, Eqs.(8,9): Missing punctuation.

    We have added punctuation to the noted equations.

18. p.10, l.5: "There is difficulty"→"There is a difficulty"

    We have amended the sentence.

19. p.10, l.7: "assumption of linearity": this is confusing here since you have not introduced the extended Kalman filter yet.

    We have removed the statement in which this phrase appears as it is not critical to the reader.

20. p.10, l.21: Even though quoting Bishop et al. (2001) [1] is certainly adequate, a reference to Hunt et al. (2007) [5] is also missing as it is equally relevant.

    We have added the reference as suggested.

21. p.10, Eq.(14) is wrong, is it? It should be

$$\mathbf{E} = \mathbf{R}^{-1/2}\mathbf{H}\mathbf{X}^{f}. \tag{1}$$

    Also it is not recommended to use $\mathbf{E}$ as it is usually used for the full ensemble matrix. Authors often use $\mathbf{S}$ instead.

    We thank the reviewer for catching this typo. We did in fact mean to define the matrix as above, as the left multiplication with its transpose is included in Eq (15). We have also changed the notation from $\mathbf{E}$ to $\mathbf{S}$ as suggested.

22. p.11, l.7: "The Kalman gain K is defined through equation (9a)": No. Not in the classical ETKF (see Hunt et al. (2007) [5]).

    We have changed the text to specify that we are following the definition of the Kalman filter as given in Bishop et al [1].

23. p.11, l.15-20: In this context, sampling errors are actually due to nonlinearity, as it was explained and proven by Bocquet et al. (2015) [2]; Raanes et al. (2019) [10].

    We have included the additional references here where we discuss the sampling errors due to nonlinearity.

24. p.11, l.25-27: "This differs to past approaches where the subspace was determined in terms of the long time averaged (invariant) unstable and neutral CLVs (Trevisan and Uboldi, 2004; Carrassi et al., 2008; Trevisan and Palatella, 2011).": This statement is misleading. You just mean that the number of retained CLVs is kept fixed. Did you?

    This is badly phrased. We meant "asymptotic Lyapunov exponents", and

therefore the rank of the error covariance matrix is kept fixed. We have updated the manuscript accordingly.

25. p.12, l.7-8: "We compute CLVs at the assimilation step using Algorithm 1.": The number of CLVs is fixed over the full time span of the algorithm, is it?

    We always compute all 9 CLVs in this case, and then only use the number corresponding to the experiment set-up in constructing the covariance matrix. In this toy model we were not as concerned with optimizing computation time. However, it is easily implemented to only compute a subset of the CLVs either specified as constant or variable based on the calculated dimension for the assimilation step. (Note, the dimension is calculated from the FTLEs computed using the QR method so this is a separate process to the CLV calculation.) We discuss more about computation time in response to the final comment (44) below.

26. p.12, l.19: "regardless of observation set" → "regardless of the observation set"

    We have amended the sentence.

27. p.12, l.23: The term "Analysis window" is unfortunate as it usually refers to the time range over which asynchronous observations are assimilated in 4D-Var or with an ensemble smoother. I guess you mean the time interval between updates. You could denote it Δt for instance. Please change it throughout the manuscript.

    We have changed "analysis window" to "assimilation window" throughout the manuscript (Δt conflicts with our integration time step notation).

28. p.13, section 5.1: Please explain better what changing the observation set has to do with the main goal of the manuscript.

    The different observation sets relate to the exploration of strongly coupled data assimilation (strong CDA), namely the use of cross-covariances to update unobserved states. We were interested in whether the use of the reduced space method (either fixed or variable) is applicable in different observation scenarios, including the cases where some subsystems are left unobserved or where there are temporally correlated errors. We have emphasized this in the introduction to the results section (Section 5) and in Section 5.1.

29. p.13, l.9-10: "We argue here that in reality, the true variance of the observation error can be spatially dependent and errors are often correlated in time.": this is a bit too much, since there are quite a few DA papers dealing with at least spatially correlated errors.

We have revised the tone of the sentence which now reads: "In many applications the true variance ..."

30. p.13, l.27: "we decrease the analysis window and do not perturb the control run at all when taking the observations.": You mean that the synthetic observations are not perturbed, do you? The sentence seems a bit twisted.

    We have amended the sentence to read: "we decrease the assimilation window and assume perfect observations."

31. p.15, l.15: "Finally we analyse our novel reduced subspace method which uses a variable number of CLVs based on the local Kaplan-Yorke dimension.": yes, but I guess you need to compute a number of CLVs corresponding to the maximum local KY dimension, so that even though it is theoretically interesting, it is, in practice, of limited interest.

    We take this as a comment. To clarify, as mentioned in our response to point 25, one only needs to compute the number of CLVs corresponding to the local Kaplan-Yorke dimension for a given assimilation step. In our experiments this varies between 0 and 8 for different assimilation steps. We discuss practical implementation in response to the reviewer's final point below.

32. p.17, Fig. 7 (a-c): please plot over a smaller range, typically [500-600] as in Fig.16.

    We have changed the range of both figures (16 and 17 in previous manuscript) to [450-550] in accordance with the discussion around the dynamical properties.

33. p.18, Table 3, and discussion around: This experiment does not account for what is actually known in the literature. You should have made an experiment with the 6 CLVs but with optimally tuned inflation, or you could have used the finite-size EnKF (Bocquet et al., 2015, and references therein). It is by now well known that the gap between the second and the third experiment might be compensated by optimally tuned inflation.

    This point was addressed in the main comments section above. With our correction to the CLV calculation, we no longer have such a discrepancy between experiments. The corrected table can be found in the following section. We have additionally done an optimization on inflation and find that the 1% is in fact optimal for these experiments.

34. p.19, l.16-18: "but we are interested if we can preserve": I don't really understand the phrase.

    We have changed the sentence to read: "we are interested to see if we

can avoid collapse (*i.e.* the loss of variability) in the ensemble mean of the extratropical attractor".

35. p.21, l.1: "in ability" → "in the ability"

    We have amended the sentence.

36. p.25, l.5-10: In this paragraph, you argue but you don't give a strong rationale for the inflation scheme you propose. You need a stronger case to convince the reader. All the more since the inflation scheme is tested with a toy model in a very specific configuration.

    We have added further discussion of the Miller *et al* [6] study to motivate our proposed modified Kalman gain. Through the study of data assimilation schemes on the Lorenz '63 model, they find that the forecast error covariance is often underestimated in highly nonlinear systems, particularly when the model is in a region of phase space subject to transitions. This leads to the Kalman gain being underestimated. The authors account for this by including the third and fourth moments of anomalies within the Kalman gain calculation, however this is done for the Extended Kalman Filter (EKF) method (see eq. 4.3 of [6]). O'Kane and Frederiksen [7] also derive a higher order gain for a closure-based statistical dynamical Kalman filter applied in spectral space (see eq. 27 of [7]). Here we use the notion that increased spread in a subsystem represents the inability of ensemble members to track the same transitions in phase space. In such a situation the forecast error covariance is likely to be underestimated (presumably due to emerging importance of higher moments), therefore we scale the forecast error covariance within the Kalman gain calculation by a factor that represents a measure of overall spread in the system. This then provides an adaptive scaling of the Kalman gain at every assimilation time step based on the background performance of the system (large spread implies an increase in Kalman gain, small spread implies a decrease). The scaling can equivalently be written as an observation error variance scaling, and its overall behaviour is a balancing between the forecast error covariance and the observation error variance within the calculation of the Kalman gain. We have expanded upon this discussion within the manuscript.

37. p.25, Eq.(25): The modified $\mathbf{P}^f$ does no have the good engineering dimensional (cube in the anomalies instead of square). What do you make of this?

    Our introduction of the scaled Kalman gain was written poorly here. We actually do not modify the forecast error covariance matrix as worded in the original manuscript. We add an additional scaling term to the forecast error covariance matrix only within the calculation of the Kalman gain. The scaling factor ($||\mathbf{P}^f||$) itself is a measure of the anomalies squared,

therefore making the quantity used in the Kalman gain a quartic measure of anomalies. In a crude way one could consider this an incorporation of higher moments into the Kalman gain, however since this is not a true estimate of the fourth moment, we used the spread-based argument for its motivation (as given above).

38. p.25, l.23-24: It seems like the β-factor approach is implementing deflation. Is it so? If yes, please use the term deflation instead of inflation, which is customary.

    We have changed the language to refer to the β-factor approach as deflation.

39. p.27, l.1: "there is remarkable"→"there is a remarkable"

    We amended the sentence.

40. p.27, l.7-8: "We have demonstrated the varying rank of the error covariance matrix related to the transient growth in the stable modes of the system.": true but this was already emphasised in the literature, so that your implicit statement of novelty should be tuned down here.

    We agree with the reviewer that our statement was too strongly worded. We have amended the sentence to read: "We have explored the varying rank of the error covariance matrix related to the transient growth in the stable modes of the system, and in particular the applicability of this varying rank on different configurations of strong CDA."

41. p.27, l.16-17: "to determine the rank": unclear and confusing; I believe you mean "to specify the appropriate rank"; you don't discover the rank, you set it.

    That is correct, we meant the connotation "to specify". We have revised the sentence accordingly.

42. p.27, l.22-24: "In particular, we found that spanning the space comprised of the asymptotic unstable, neutral, and first weakly stable mode (5 CLVs in this case) performed much worse than using either dimension measure (asymptotic and local).": I don't think so. This is one weak point of your study. It is known that in this case, the inflation must be adjusted to account for the error upscaling from the the region of the spectrum (Grudzien et al., 2018a,b). I don't believe that you have tuned the inflation, have you? If true, your statement appears to be too strong.

    We have toned down the language around the discussion of these results after the correction to the calculation. We no longer claim the 5 CLV case performs "much" worse, as all methods now perform comparably. We

point out, however, that the 6 CLV and variable CLV both show a reduction in the full RMSE which can be related to significant linear growth in more than one stable mode. We also have included the reference [4] within our discussion of inflation in Section 4.1, and the reference [3] in discussing the impact of transient growth of asymptotically stable modes on model errors in the introduction.

43. p.28, l.19-20: "The adaptive scaling introduced here can be applied to general systems with weak coupling, although care may need to be taken in the choice of the norm.": No, you have not proven anything like that. Please remove the statement.

    Instead of removing, we have amended the statement to one which reflects our original sentiment. We wanted to suggest that the method be tested on other systems of weak coupling and then perhaps a more general statement can be made under deeper analysis. We have changed the statement to read "The adaptive scaling introduced here should be tested on additional systems with weak coupling in order to assess its general applicability, although care may need to be taken in the choice of the norm."

44. p.28, l.33-34: "Future work should also consider the numerical cost of CLV calculation and methods to increase efficiency for high dimensional systems": At the very end, you raise what experts familiar with AUS have in mind reading your paper: what you propose is certainly interesting and of theoretical interest but of lesser practical value since (i) one needs to compute the CLVs alongside (ii) with the variable CLV context, you need to compute the maximum number of CLVs. You should mentioned this point way earlier in the paper, unless I am mistaken.

    The reviewer is correct in that we do not address computational cost throughout the paper. This was mainly intentional, as we did not aim to optimize computational performance, but rather explore a method that allows for the reduction of phase space and/or better representation of errors in that reduced subspace. Whether or not there can be a computational cost reduction by using this method over spanning the space needed to fully sample the variance is a question we do not attempt to answer as it will depend on the system one wishes to assimilate. In accordance with the reviewer's request, we have added a footnote within the introduction at the point where we discuss assimilation in the unstable subspace (AUS). The footnote acknowledges the additional cost that comes with computing the unstable subspace which may or may not be less than the cost of sampling the full model variance, and it also states that we will leave the exploration of numerical efficiency in high dimensional systems for future study.

    We additionally note that the projection onto CLVs is an example of one

specific projection that works for the variable local dimension, but it is not the only one. One could also project onto the backwards Lyapunov vectors (BLVs) which are computationally less expensive to compute and attain similar results. Table 2 in the revised manuscript includes the results of variable dimension and projection onto BLVs. We have added a discussion of this alternate projection into the manuscript, as well as the additional statistics of the variable BLV experiment. However, we focus on the CLVs in this study as the *a posteriori* analysis of CLV alignment can provide more information of the time-varying phase space behaviour. (The BLVs are orthogonal by construction.) The revised manuscript has an additional discussion of CLV alignment, variable dimension, and specifically the relationship to ensemble data assimilation which justifies the utility of CLVs.

We imagine that it could be possible to find a computationally efficient projection for high dimensional systems that incorporates the variable dimension aspect. Our main goal in this manuscript though was to introduce the implementation of time-varying dimension in this toy model with different observational sets to understand in what configurations one might expect successful results. It would be of interest for practical applications if future studies could explore numerically efficient projections that span the time-varying dimension and therefore utilise the ideas of AUS in high dimensional systems.

SUMMARY OF MAJOR MANUSCRIPT CHANGES

"pg" refers to page number in following latexdiff document

Section 1	pg 2	Added footnote discussing cost of computing unstable/neutral manifold
	pg 2	Additional relevant references [3, 4]
Section 2.2	pg 7	Introduction and discussion of concept of local dimension used throughout manuscript
Section 3	pg 7	Explanation of cocycle and mathematical formulation used
	pg 9	Comparison of calculating FTLEs as growth rates of backwards or covariant Lyapunov vectors
	pg 10	Additional figure comparing local KY measure calculated from FTBLEs or FTCLEs (Fig 6)
Sections 4.1	pg 12	Corrected equation 14
	pg 12	Additional references and discussion regarding use of inflation in DA of nonlinear systems
Section 4.2	pg 13	Discussion of CLV alignment and local dimension measure in context of DA
	pg 14	Additional figure comparing CLV alignment at two different times (Fig 7)
Section 5	pg 14	Justification for considering different observational sets
	pg 15	More detailed description of how the dynamical properties are calculated within the DA experiments
Section 5.2	pg 16	Discussion of using BLVs in place of CLVs
	pg 17	Clarified definitions of metrics and removed MAD as it is not discussed
	pg 17	Updated RMSE values in Table 2 from corrected experiments
	pg 17	Added statistics for BLV experiment
Section 5.3	pg 21	Removed figure of DA experiments with atmosphere observations
	pg 21	Corrected Table 3 and the discussion of the experiments
Section 5.4	pg 23	Updated RMSE values in Table 2 from corrected experiments
Section 5.5	pg 26	Updated RMSE and inflation values in Table 2 from corrected experiments
Section 5.6	pg 26	Additional justification for adaptive Kalman gain scheme
	pg 27	Defined scheme in terms of Kalman gain scaling rather than forecast covariance scaling
	pg 28	Showed the variable CLV experiment in Figure 12 rather than the 9 CLV
	pg 29	Added statistics of variable CLV experiments to Table 6
Section 6	pg 28-30	Generally softened our tone in discussion of results
	pg 31	Additional paragraph discussing the adaptive Kalman gain scheme and the need for an analysis of general applicability

References

[1] Craig H Bishop, Brian J Etherton, and Sharanya J Majumdar. Adaptive sampling with the ensemble transform kalman filter. part i: Theoretical aspects. *Monthly weather review*, 129(3):420–436, 2001.

[2] Marc Bocquet, Patrick N Raanes, and Alexis Hannart. Expanding the validity of the ensemble kalman filter without the intrinsic need for inflation. *Nonlinear Processes in Geophysics*, 22(6):645–662, 2015.

[3] Colin Grudzien, Alberto Carrassi, and Marc Bocquet. Asymptotic forecast uncertainty and the unstable subspace in the presence of additive model error. *SIAM/ASA Journal on Uncertainty Quantification*, 6(4):1335–1363, 2018.

[4] Colin Grudzien, Alberto Carrassi, and Marc Bocquet. Chaotic dynamics and the role of covariance inflation for reduced rank kalman filters with model error. *Nonlinear Processes in Geophysics*, 25(3):633–648, 2018.

[5] Brian R Hunt, Eric J Kostelich, and Istvan Szunyogh. Efficient data assimilation for spatiotemporal chaos: A local ensemble transform kalman filter. *Physica D: Nonlinear Phenomena*, 230(1-2):112–126, 2007.

[6] Robert N Miller, Michael Ghil, and Francois Gauthiez. Advanced data assimilation in strongly nonlinear dynamical systems. *Journal of the atmospheric sciences*, 51(8):1037–1056, 1994.

[7] Terence O'Kane and Jorgen Frederiksen. Comparison of statistical dynamical, square root and ensemble kalman filters. *Entropy*, 10(4):684–721, 2008.

[8] Luigi Palatella and Anna Trevisan. Interaction of lyapunov vectors in the formulation of the nonlinear extension of the kalman filter. *Physical Review E*, 91(4):042905, 2015.

[9] M Peña and E Kalnay. Separating fast and slow modes in coupled chaotic systems. *Nonlinear Processes in Geophysics*, 11(3):319–327, 2004.

[10] Patrick N Raanes, Marc Bocquet, and Alberto Carrassi. Adaptive covariance inflation in the ensemble kalman filter by gaussian scale mixtures. *Quarterly Journal of the Royal Meteorological Society*, 145(718):53–75, 2019.

[11] Takuma Yoshida and Eugenia Kalnay. Correlation-cutoff method for covariance localization in strongly coupled data assimilation. *Monthly Weather Review*, 146(9):2881–2889, 2018.

Application of local attractor dimension to reduced space strongly coupled data assimilation for chaotic multiscale systems

Courtney Quinn[1], Terence J. O'Kane[1], and Vassili Kitsios[1]

[1]Decadal Climate Forecasting Project, CSIRO Oceans and Atmosphere, Hobart, TAS, AU

Correspondence: Courtney Quinn (courtney.quinn@csiro.au)

Abstract. The basis and challenge of strongly coupled data assimilation (CDA) is the accurate representation of cross-domain covariances between various coupled subsystems with disparate spatio-temporal scales, where often one or more subsystems are unobserved. In this study, we explore strong CDA using ensemble Kalman filtering methods applied to a conceptual multiscale chaotic model consisting of three coupled Lorenz attractors. We introduce the use of the local attractor dimension (i.e. the Kaplan-Yorke dimension, $\dim_{KY}$) to ~~determine~~ prescribe the rank of the background covariance matrix which we construct using a variable number of weighted covariant Lyapunov vectors (CLVs). Specifically, we consider the ability to track the nonlinear trajectory of each of the subsystems with different variants of sparse observations, relying only on the cross-domain covariance to determine an accurate analysis for tracking the trajectory of the unobserved subdomain. We find that spanning the global unstable and neutral subspaces is not sufficient at times where the nonlinear dynamics and intermittent linear error growth along a stable direction combine. At such times a subset of the local stable subspace is also needed to be represented in the ensemble. In this regard the local $\dim_{KY}$ provides an accurate estimate of the required rank. Additionally, we show that spanning the full space does not improve performance significantly relative to spanning only the subspace determined by the local dimension. Where weak coupling between subsystems leads to covariance collapse in one or more of the unobserved subsystems, we apply a novel modified Kalman gain where the background covariances are scaled by their Frobenius norm. This modified gain increases the magnitude of the innovations and the effective dimension of the unobserved domains relative to the strength of the coupling and time-scale separation. We conclude with a discussion on the implications for higher dimensional systems.

1 Introduction

As the world of climate modelling has moved towards coupled Earth system models which combine ocean, atmosphere, sea-ice, and biogeochemical effects, it is essential to understand how the respective domains of disparate spatio-temporal scales covary and influence each other. In the context of state estimation, strongly coupled data assimilation (CDA) in multiscale systems allows the quantification of cross-domain dynamics. Specifically, strong CDA uses the cross-covariances amongst all components to influence the analysis increment, meaning that unobserved subsystems are directly adjusted in the analysis step regardless of observation set and coupling strengths (Laloyaux et al., 2016; O'Kane et al., 2019). Strong CDA has shown the potential to outperform weakly coupled or uncoupled approaches in intermediate complexity atmosphere-ocean systems

(Sluka et al., 2016; Penny et al., 2019), however CDA has the additional requirements of increased ensemble sizes (Han et al., 2013) and well observed state (prognostic) variables (Kang et al., 2011). Ensemble DA methods rely on properly sampling the variance of the model, implying that very large ensemble sizes are needed for high dimensional systems. In practical implementation this is often not possible due to computational costs and limitations. It is therefore necessary to investigate and develop new methods of accurately representing error growth in multiscale systems.

One approach to reduce the requirement to adequately sample the background covariances is to perform CDA in the reduced subspace of the unstable modes, known as assimilation in the unstable subspace (AUS) [1] (Trevisan and Uboldi, 2004; Carrassi et al., 2007; Trevisan et al., 2010; Trevisan and Palatella, 2011; Palatella et al., 2013; Bocquet and Carrassi, 2017). The concept behind AUS methods is that the analysis increment should lie in the unstable and neutral subspaces of the model, therefore retaining the spatial structure of dominant instabilities (Trevisan and Uboldi, 2004). Many implementations of AUS involve variational data assimilation methods, namely finding the model trajectory which best fits observations through solving an optimization cost function. On the other hand, the widely used ensemble Kalman filtering methods have been shown to best capture the unstable error growth in nonlinear systems (Evensen, 1997). For this reason, we focus on the ability to accurately represent the unstable and neutral subspace within the ensemble Kalman filtering framework.

The main motivation for this study comes from the conjecture that when applying ensemble Kalman filtering methods to high dimensional nonlinear systems, the true time-dependent error covariance matrix collapses onto a subspace of the model domain which contains unstable, neutral, and sometimes weakly stable modes. While previous results prove the collapse of the error covariance matrix onto the unstable and neutral subspace for linear systems (Gurumoorthy et al., 2017; Bocquet et al., 2017), nonlinear systems have the additional complication that the unstable subspace is a function of the underlying trajectory and not globally defined (Bocquet et al., 2017). As nonlinearity increases, short-term dynamics can cause some stable modes of the linearized system to experience significant growth. These additional modes are therefore important when considering local error growth in ensemble DA methods~~(Ng et al., 2011)~~. While this has previously been addressed in the context of perfect nonlinear models (Ng et al., 2011), recent studies have shown that the additional transient unstable modes can also further amplify perturbations in the presence of model error (Grudzien et al., 2018a, b).

Such transient error growth has previously been explored in ocean-atmosphere models of varying complexity. One way of quantifying local error growth is through finite-time Lyapunov exponents (FTLEs), *i.e.* rates of expansion and contraction over finite intervals of time. Nese and Dutton (1993) utilised the largest (leading) FTLE to quantify predictability times along different parts of the attractor of a low-order ocean-atmosphere model. The statistical properties of FTLEs have been studied more recently in a range of atmosphere and ocean models with varying complexity, including low-order models (Vannitsem, 2017) and intermediate-complexity models (Vannitsem, 2017; De Cruz et al., 2018; Kwasniok, 2019). While FTLEs provide local rates of error growth, one can also consider directions of local error growth. Early work in this area considered finite-time normal modes, which are generalised as the eigenvectors of tangent linear propagators over a given time interval, and studied

[1] There is a computational cost accompanying the determination of the unstable and neutral subspaces which may or may not be less than the cost of adequately sampling the model covariances. We do not attempt to comment on numerical efficiency of AUS methods applied to high dimensional systems. The exploration of cost-effective methods for determining the reduced subspace is left for future study.

their relation to blocking events in the atmosphere (Frederiksen, 1997, 2000; Wei and Frederiksen, 2005). More recent studies have focused on covariant Lyapunov vectors (CLVs) which give directions of asymptotic growth and decay in the tangent linear space. While these vectors have an average growth rate corresponding to the asymptotic Lyapunov exponents, their finite-time behaviour may differ. This finite-time behaviour of CLVs has been analysed across a range of quasi-geostrophic atmosphere (Schubert and Lucarini, 2015, 2016; Gritsun and Lucarini, 2017) and coupled atmosphere-ocean (Vannitsem and Lucarini, 2016) models.

In this study we utilise FTLEs and CLVs within the ensemble Kalman filtering framework applied to a low-dimensional chaotic model with spatio-temporal scale separation. The model was designed to represent the interaction between the ocean, extratropical atmosphere, and an ocean-atmosphere interface (referred to as the tropical atmosphere). The idea is that the ocean and extratropical atmosphere are only implicitly coupled through the interface, with the interface being strongly coupled to the ocean and weakly coupled to the extratropical atmosphere. We consider the performance of strong CDA on this paradigm model with different subsets of observations. We introduce the use of ~~local~~ a varying number of CLVs to form the forecast error covariance matrix. The idea of AUS is incorporated through the use of ~~a~~ the time-varying subspace defined by the local attractor dimension. The dimension is calculated through FTLEs and the error covariance matrix is constructed via a projection of the ensemble members onto a corresponding subset of the CLVs at each analysis step. We compare full rank ensemble transform and square-root filters to “phase space" variants whose background covariances are defined in terms of either the ~~local or global~~ finite-time or asymptotic attractor dimension. Another variant considered includes only the unstable, neutral, and weakest stable CLVs. We consider benchmark calculations comparing to the recent work of Yoshida and Kalnay (2018) and then a comprehensive set of experiments where the various domains are partially or even completely unobserved. ~~We also examine the role of correlated versus random observational errors.~~

The paper is organized as follows. Section 2 introduces the paradigm model and discusses the dynamical properties of a control simulation. Section 3 describes the method for calculating the CLVs and discusses the possibility of CLV alignment. Section 4 summarizes the Kalman filtering method and introduces the modification to the calculation of the error covariance matrix. The configurations and results of the DA experiments are presented in Section 5~~, along with a novel scheme for adaptive Kalman gain inflation~~. The implications of the results of this study and future endeavours are discussed in Section 6.

2 Coupled Lorenz model for global circulation

2.1 Peña and Kalnay model

This section describes a low-dimensional chaotic model representing a coupled ocean and atmosphere. It is a system of three coupled Lorenz 63 models introduced by Peña and Kalnay (2004) to study unstable modes with a time scale separation. This model has previously been described in modified form by Norwood et al. (2013) who used it to investigate the instability properties of related dynamical vectors i.e. bred vectors (BVs), singular vectors (SVs) and CLVs, and by Yoshida and Kalnay

(2018) and O'Kane et al. (2019) in the context of strongly coupled data assimilation. The model is given as follows:

$$\dot{x}_e = \sigma(y_e - x_e) - c_e(Sx_t + k_1), \tag{1a}$$

$$\dot{y}_e = \rho x_e - y_e - x_e z_e + c_e(Sy_t + k_1), \tag{1b}$$

$$\dot{z}_e = x_e y_e - \beta z_e, \tag{1c}$$

$$\dot{x}_t = \sigma(y_t - x_t) - c(SX + k_2) - c_e(Sx_e + k_1), \tag{1d}$$

$$\dot{y}_t = \rho x_t - y_t - x_t z_t + c(SY + k_2) + c_e(Sy_e + k_1), \tag{1e}$$

$$\dot{z}_t = x_t y_t - \beta z_t + c_z Z, \tag{1f}$$

$$\dot{X} = \tau\sigma(Y - X) - c(x_t + k_2), \tag{1g}$$

$$\dot{Y} = \tau\rho X - \tau Y - \tau SXZ + c(y_t + k_2), \tag{1h}$$

$$\dot{Z} = \tau SXY - \tau\beta Z - c_z z_t. \tag{1i}$$

The model is proposed as representing the fast extratropical atmosphere (1a-c), fast tropical atmosphere (1d-f), and slow tropical ocean (1g-i). The standard Lorenz parameter values of $\sigma = 10$, $\rho = 28$, and $\beta = 8/3$ are used. The coupling coefficients are $c_e = 0.08$ and $c = c_z = 1$, representing a weak coupling of extratropical to tropical atmosphere and a strong coupling of tropical atmosphere and ocean. The scaling parameters are set as $\tau = 0.1$ and $S = 1$, giving an explicit timescale separation (note there is still difference in the spatial scales through the dynamics). The parameters $k_1 = 10$ and $k_2 = -11$ are chosen as uncentering parameters.

More generally, these choices lead to a tropical subsystem that is dominated by changes in the ocean subsystem, but has an extratropical atmosphere, representative of weather noise, whose behaviour is similar to the original Lorenz model in that the system exhibits chaotic behaviour with two distinct regimes observed in the x_e and y_e coordinates of the extratropical atmosphere. The ocean exhibits significant deviations from its normal trajectory about every 2-8 years where three years corresponds to approximately 10 time units. Figure 1 shows typical trajectories of the x_e, x_t, and X components of the extratropical, tropical, and ocean subsystems respectively. Figure 2 shows the approximate phase space structure of each of the respective subsystem's attractor.

2.2 Lyapunov exponents and dimension

We are interested in analysing both the ~~local and global~~ short-term and asymptotic dynamics of system (1). We start by considering the asymptotic behaviour of trajectories, which can be understood through the Lyapunov exponents. Chaotic systems are characterized by one or more positive Lyapunov exponents (Benettin et al., 1976; Sano and Sawada, 1985), and the underlying attractor dimension can be related to the values of the Lyapunov exponents (Young, 1982; Eckmann and Ruelle, 1985).

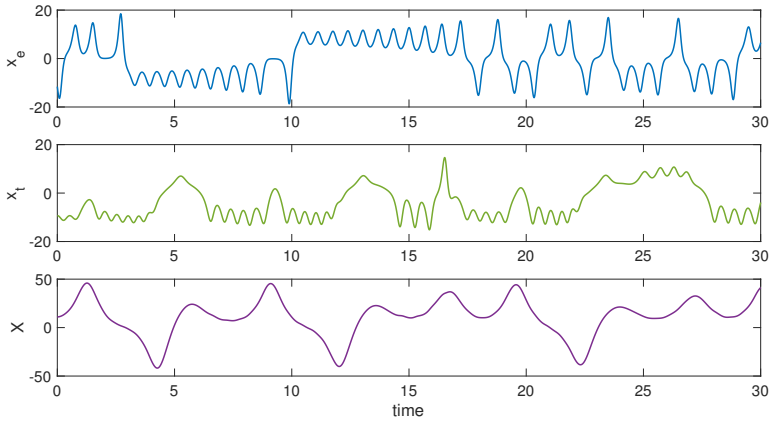

Figure 1. Example trajectories of coupled Lorenz model (1) for x_e (top), x_t (middle), and X (bottom).

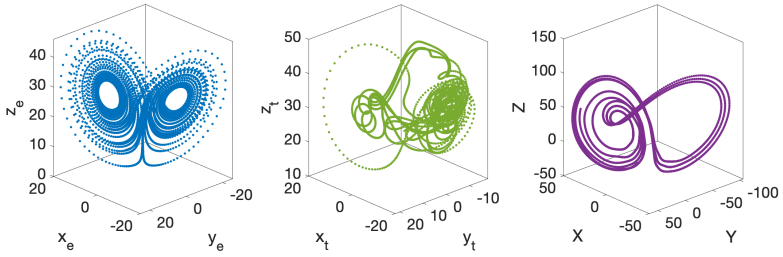

Figure 2. Trajectories along attractors of the extratropical (left), tropical (middle) and ocean (right) subsystems of (1).

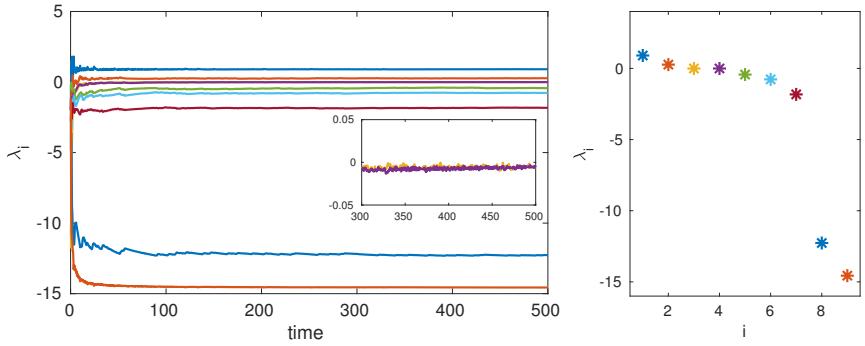

Figure 3. (Left) Convergence of Lyapunov exponents of (1) with inset of zoom around zero to show the two neutral exponents. (Right) Asymptotic values of Lyapunov exponents of (1).

We compute the Lyapunov exponents using a QR decomposition method (see *e.g.* Dieci et al. (1997)). For the computation we run the model for 1000 time units to ensure convergence onto the attractor. We use a time step of 0.01 and compute the Lyapunov exponents from the last 500 time units, with an orthonormalization time step of 0.25 for the QR method. The convergence of the Lyapunov exponents is shown in Figure 3. We observe that for these parameter values there are two unstable and two approximately neutral Lyapunov exponents. We list the values of all nine computed asymptotic exponents in Table 1.

λ_1	λ_2	λ_3	λ_4	λ_5	λ_6	λ_7	λ_8	λ_9
0.9071	0.2670	-0.0056	-0.0060	-0.4326	-0.7706	-1.8263	-12.2691	-14.5640

Table 1. Asymptotic Lyapunov exponents of (1) computed over 500 time units using a QR decomposition method, time step of 0.01, and orthogonalization step of 0.25.

Given the approximated asymptotic Lyapunov exponents in Table 1, we can compute the global attractor dimension i.e. the number of active degrees of freedom. Notice that there is a large spectral gap between the seventh and eighth Lyapunov exponents. This gives evidence that the effective dimension of the attractor will be less than 8. Throughout this study we will use the Kaplan-Yorke dimension (Kaplan and Yorke, 1979; Frederickson et al., 1983) to calculate the upper bound on attractor dimension. It is defined as follows:

$$\dim_{KY} := j + \frac{\sum_{i=1}^{j} \lambda_i}{|\lambda_{j+1}|}, \tag{2}$$

where j is the largest integer such that

$$\sum_{i=1}^{j} \lambda_i \geq 0$$

and

$$\sum_{i=1}^{j+1} \lambda_i < 0.$$

In addition we calculate the Kolmogorov–Sinai entropy ent_{KS} as a measure of the diversity of the trajectories generated by the dynamical system and determined through the Pesin formula

$$\mathrm{ent}_{KS} = \sum_{\lambda>0} \lambda_i, \tag{3}$$

which provides an upper bound to ~~ent_{KS}~~ the entropy (Eckmann and Ruelle, 1985).

With the values in Table 1 we obtain a value of 5.9473 for the global attractor dimension of the 9-component system. As previously mentioned, asymptotically stable modes can experience transient periods of linear unstable growth. We therefore define local dimension through the computation of (2) using finite-time Lyapunov exponents (FTLEs). The computation of FTLEs is similar to that of the asymptotic Lyapunov exponents, with the difference being a finite window of time over which the exponents are computed. The FTLEs then serve as a time-dependent measure of the local unstable, neutral, and stable growth rates of the evolving system (Abarbanel et al., 1991; Eckhardt and Yao, 1993; Yoden and Nomura, 1993). The temporal

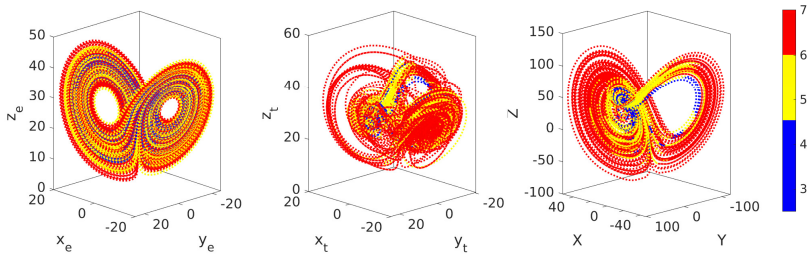

Figure 4. Local Kaplan-Yorke dimension plotted along trajectory in phase space for the extratropical atmosphere (left), tropical atmosphere (middle), and ocean (right) subsystems.

variability of FTLEs is highly dependent on the window size, τ, over which they are computed. As $\tau \to \infty$ the variability reduces and the FTLEs approach ~~their corresponding asymptotic~~ the asymptotic Lyapunov exponent values (Yoden and Nomura, 1993). We compute the FTLEs for a window size $\tau = 4$ and the corresponding time-varying Kaplan-Yorke dimension ~~.~~ which we will refer to as a "local" dimension. This will give a measure which reflects variations in the finite-time growth rates, with higher (lower) dimension signifying increased instability (stability) in the FTLEs. More specifically this is an upper bound on the true local dimension - the measure does not take into account the geometric degeneracy which can occur when many of the leading CLVs can become aligned. In practice this overestimation of dimension is actually beneficial within the DA framework (more discussion on this can be found in Section 4.2).

Figure 4 shows the local dimension plotted along the attractors of each of the subsystems. We see that the local dimension is lowest when the model is in the interior region of the ocean subsystem attractor. In contrast, the extratropical atmosphere subsystem attractor displays periods of low dimension largely uniformly confined to the center of each lobe of the attractor. The tropical atmosphere also shows most of the measures of low dimension confined to the interior of the attractor, reflecting the strong ocean coupling.

3 Covariant Lyapunov vectors

The existence of Lyapunov vectors for a large class of dynamical systems was proven by Oseledets (1968). The Multiplicative Ergodic Theorem states that there exists a relation between Lyapunov exponents, λ_i, and a (non-unique) set of vectors $\boldsymbol{\phi}$ such that

$$\lambda_i = \lim_{\tau \to \infty} \frac{1}{\tau} \log ||\mathcal{A}(x(t), \tau)\boldsymbol{\phi}|| \qquad \text{iff} \qquad \boldsymbol{\phi} \in \Phi_i(x(t)) \setminus \Phi_{i+1}(x(t)) \tag{4}$$

Here, ~~$\mathcal{A}(x(t), \tau)$ forms the cocycle of~~ $\mathcal{A}(x(t), \tau)$ is the forward and backward mapping of solutions under the tangent dynamics ~~for~~ of a given dynamical system ~~.~~ (also referred to as the cocycle). For system (1), $\mathcal{A}(x(t), \tau) = \mathrm{e}^{\tau J f(x(t))}$ where Jf denotes the Jacobian of f, the right-hand-side of system (1). The subspaces (Φ_i) on which the growth rates (λ_i) occur are covariant with the tangent dynamics and invariant under time reversal (Ginelli et al., 2007; Froyland et al., 2013). The covariant Lyapunov vectors (CLVs) are then defined as the set of directions at each point in phase space that satisfy (4) both backwards and forwards in time

(Ginelli et al., 2007; Ng et al., 2011). In the last few decades there have been significant advances in the ability to numerically approximate such vectors for chaotic dynamical systems (Ginelli et al., 2007; Wolfe and Samelson, 2007; Froyland et al., 2013). In this work we will employ a numerical algorithm introduced by Froyland et al. (2013) (Algorithm 2.2 in the aforementioned study). We summarize this algorithm below.

Algorithm 1 Summary of numerical algorithm for calculating CLVs introduced by Froyland et al. (2013)

1. Construct matrix cocycle $\mathcal{A}(x^{i+m},0)$ for every ~~$i \in [-N,...,N]$~~ $m \in [-N,...,N]$.
2. Compute the eigenvectors $\boldsymbol{e}_j^{i-N}$ of $\mathcal{A}(x^{i-N},N)^*\mathcal{A}(x^{i-N},N)$ [the right singular vectors of $\mathcal{A}(x^{i-N},N)$], where $\mathcal{A}(x^{i-N},N) = \mathcal{A}(x^i,0)\cdot...\cdot\mathcal{A}(x^{i-N},0)$. Note that $\mathcal{A}(x^{i-N},N)^*$ is the adjoint of $\mathcal{A}(x^{i-N},N)$.
3. Push forward by multiplication of matrix cocycle, $\boldsymbol{\phi}_j^i = \mathcal{A}(x^{i-N},N)\boldsymbol{e}_j^{i-N}$.
4. For each j, reorthogonalize $\boldsymbol{\phi}_j^i$ with subspace spanned by eigenvectors $\boldsymbol{e}_k^{i-n}$ for $k = 1,...,j-1$ of $\mathcal{A}(x^{i-n},N)^*\mathcal{A}(x^{i-n},N)$ every n time steps.
5. The vector $\boldsymbol{\phi}_j^i$ is then an approximation of the $j-th$ largest CLV at time $t = t_i$.

It should be mentioned that the push forward step need not be equal to N; $M \neq N$ for $\mathcal{A}(x^{i-N},M)$. However, for all calculations in this study we consider only the case $M = N$. The trajectory of the system is discretized with time step Δt such that $x^i = x(t_i)$ and $x^{i+m} = x(t_i + m\Delta t)$.

We examine the effectiveness of this algorithm on the Peña and Kalnay (2004) model introduced in Section 2. By definition, CLVs describe the directions in phase space corresponding to different growth rates. Two or more CLVs can align during a transition to a different regime in phase space. We calculate the alignment through

$$\theta_{i,j} = \frac{|\boldsymbol{\phi}_i \cdot \boldsymbol{\phi}_j|}{||\boldsymbol{\phi}_i|| \cdot ||\boldsymbol{\phi}_j||}. \tag{5}$$

Here, $\theta_{i,j} = |\cos(\Theta_{i,j})|$ where $\Theta_{i,j}$ is the angle between the i-th and j-th CLV. Larger values of $\theta_{i,j}$ imply alignment of the two CLVs. Figure 5 shows the alignment of the unstable CLVs ($\theta_{1,2}$) and the neutral CLVs ($\theta_{3,4}$) plotted against the X component of system (1), along with the FTLEs and corresponding local time-varying Kaplan-Yorke dimension. ~~As the changes in local dimension reflect the structure of the ocean subsystem~~ Since the window to calculate the FTLEs was chosen based on the variability timescales of the ocean subsystem, the subsequent local dimension measure should reflect areas of increased or decreased instabilty along the ocean attractor (Figure 4)~~, we~~ . We also expect alignment of the CLVs during a transition in this subsystem. The CLVs analysed in Figure 5 are calculated from the first 35 time units of the previous model run with a time step $\Delta t = 0.01$. We start the calculation at $t = 5$ to allow for initialization and a window size of $\tau = 4$. The parameters for the algorithm are set as $N = 400$ and $n = 25$. It can be seen that the algorithm detects near alignment of either the unstable or neutral CLVs during the transitions in the ocean subsystem. The transitions here are between the inner part of the attractor with smaller oscillation amplitudes and the outer, large amplitude excursions. In general, the alignment is most prominent in the outer, large amplitude part of the attractor. This follows the changes in local dimension, shown in the lower panel of Figure 5. Higher local dimension tends to accompany alignment of the unstable and neutral CLVs. This relates to the inability of the Kaplan-Yorke dimension measure to account for finite-time geometric degeneracy.

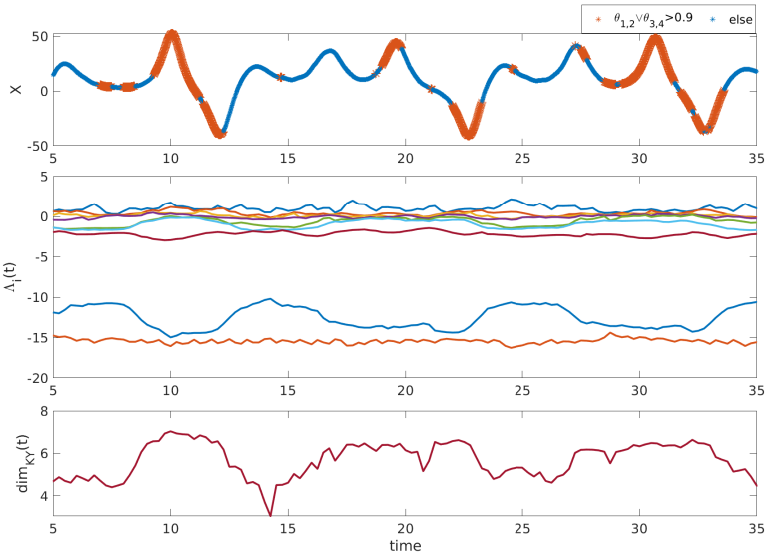

Figure 5. Local dynamical properties of a segment of an example model run. (Top) Alignment of CLVs associated with the unstable and neutral subspaces plotted along the x-coordinate of the ocean subsystem. Large orange stars indicate high alignment of unstable or neutral CLVs ($\theta_{1,2} > 0.9$ or $\theta_{3,4} > 0.9$). (Middle) Time-varying FTLEs $\Lambda_i(t)$ computed over window $\tau = 4$. (Bottom) Local Kaplan-Yorke dimension calculated from FTLEs.

At this point we will comment on the non-trivial relationship between the CLVs and FTLEs calculated here. As discussed in Vannitsem and Lucarini (2016), there are three different types of FTLEs one can compute: backward (FTBLEs), forward (FTFLEs), and covariant (FTCLEs). Each type of FTLE gives the local growth rate of the corresponding Lyapunov vectors. Although all three converge to the asymptotic Lyapunov exponents as the computation window increases, the temporal variability for finite window size can be different depending on the model at hand. Vannitsem and Lucarini found that when calculating the growth rates of the CLVs, higher variability in the FTCLEs corresponding to neutral or near-zero modes occurred compared to the other two methods. This could have implications on the local Kaplan-Yorke dimension if one were to use the FTCLEs rather than the FTBLEs in the calculation. We remark here that the QR method produces backward Lyapunov vectors (BLVs) and their corresponding FTBLEs. We therefore compare the Kaplan-Yorke dimension as computed from FTCLEs and FTBLEs for the coupled Lorenz system (1) in Figure 6. We see that for this model the dimension calculated from FTBLEs approximately bounds that calculated from FTCLEs. Since we will be using the local Kaplan-Yorke dimension as a lower bound within the framework of our experiments, the FTBLEs give a conservative estimate of dimension that is varying with our dynamics (see section 4.2 for discussion of the implementation of dimension into our experiments).

In the following sections, we will utilise CLVs within the data assimilation framework of ensemble forecasting. The CLVs will be used to construct the forecast error covariance matrix, which informs the increment used on ensemble members to bring them closer to observations. Using CLVs in this context suggests a more accurate method of forming the forecast error covariance matrix when the true covariance is undersampled due to insufficient number of ensemble members (see *e.g.*

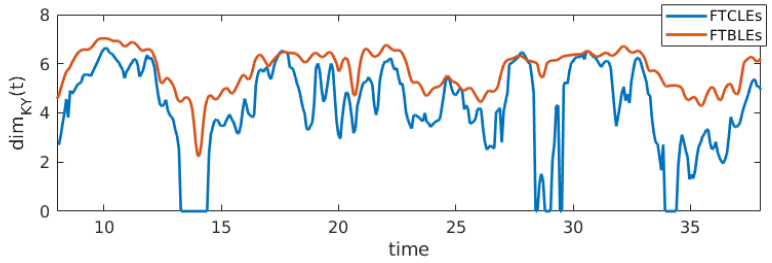

Figure 6. Comparison of finite-time Kaplan-Yorke dimension calculated using the growth rates of CLVs (FTCLEs) and the QR method (FTBLEs).

Palatella and Trevisan (2015) where the authors applied a similar approach using BLVs on the classical Lorenz (1963) and Lorenz (1996) systems).

4 Data assimilation with the Kalman filter

We now summarize the Kalman filter equations. For detailed derivations we refer the interested reader to the reviews by Evensen (2003), Houtekamer and Zhang (2016) or Carrassi et al. (2018). Here we follow the notation of Carrassi et al. (2018). Consider a deterministic or stochastic model defined by

$$\boldsymbol{x}_k = \mathcal{M}_{k:k-1}(\boldsymbol{x}_{k-1}, \boldsymbol{p}) + \eta_k, \tag{6}$$

where $\boldsymbol{x}_k \in \mathbb{R}^N$ is the model state at time $t = t_k$, $\boldsymbol{p} \in \mathbb{R}^p$ are the model parameters, $\mathcal{M}_{k:k-1} : \mathbb{R}^N \to \mathbb{R}^N$ is a function taking the model from time t_{k-1} to t_k, and η_k is the model error at time t_k (for deterministic systems let $\eta_k = 0$). Suppose that there exists a time-dependent set of observations $\boldsymbol{y} \in \mathbb{R}^d$ which can be expressed as a function of the model state through

$$\boldsymbol{y}_k = \mathcal{H}_k(\boldsymbol{x}_k) + \epsilon_k. \tag{7}$$

The observation operator $\mathcal{H}_k : \mathbb{R}^N \to \mathbb{R}^d$ can be linear or nonlinear, and ϵ_k is the observational error.

In the Kalman filter method, equations (6) and (7) are assumed to be linear, resulting in evolution and observation matrices $\mathbf{M}_{k:k-1}$ and $\mathbf{H}_k$ respectively. The model and observation errors, η_k and ϵ_k, are taken to be uncorrelated in time (white noise) and from a Gaussian distribution with covariance matrices $\mathbf{Q}_k \in \mathbb{R}^{N\times N}$ and $\mathbf{R}_k \in \mathbb{R}^{d\times d}$ respectively. There are two basic steps to the Kalman filter method: forecast and analysis.

– **Forecast equations**

$$\boldsymbol{x}_k^f = \mathbf{M}_{k:k-1}\boldsymbol{x}_{k-1}^a, \tag{8a}$$

$$\mathbf{P}_k^f = \mathbf{M}_{k:k-1}\mathbf{P}_{k-1}^a\mathbf{M}_{k:k-1}^{\mathrm{T}} + \mathbf{Q}_k. \tag{8b}$$

– **Analysis equations**

$$\mathbf{K}_k = \mathbf{P}_k^f \mathbf{H}_k^{\mathrm{T}} [\mathbf{H}_k \mathbf{P}_k^f \mathbf{H}_k^{\mathrm{T}} + \mathbf{R}_k]^{-1}, \tag{9a}$$

$$\boldsymbol{x}_k^a = \boldsymbol{x}_k^f + \mathbf{K}_k(\boldsymbol{y}_k - \mathbf{H}\boldsymbol{x}_k^f), \tag{9b}$$

$$\mathbf{P}_k^a = (\mathbf{I}_k - \mathbf{K}_k \mathbf{H}_k)\mathbf{P}_k^f. \tag{9c}$$

There is ~~difficulty in implementing~~ a difficulty in finding accurate solutions to equations (8-9) for realistic systems which have high dimension and are nonlinear (as is the case in weather and climate forecasting). ~~Solving such equations are computationally expensive and produce errors from the assumption of linearity (Evensen, 1994).~~ Within the Kalman filter class, various ensemble filter variants have been applied to tracking trajectories in nonlinear systems. The most popular are the deterministic filters (Tippett et al., 2003; Sakov and Oke, 2008; Sakov et al., 2012).

4.1 Ensemble Kalman filtering

Ensemble Kalman filtering methods use Monte Carlo sampling to form the approximate error statistics of a model. An ensemble of model states $\boldsymbol{x}^f \in \mathbb{R}^N$ with a finite number of ensemble members m produces an approximation to the true error covariance matrix as follows. The ensemble forecast anomaly matrix $\mathbf{X}^f \in \mathbb{R}^{N \times m}$ is constructed with respect to the ensemble mean $\overline{\boldsymbol{x}}^f \in \mathbb{R}^N$:

$$\overline{\boldsymbol{x}}^f = \frac{1}{m} \sum_{n=1}^{m} \boldsymbol{x}_n^f, \tag{10a}$$

$$\mathbf{X}^f \equiv \frac{1}{\sqrt{m-1}} \left[\boldsymbol{x}_1^f - \overline{\boldsymbol{x}}^f, \ldots, \boldsymbol{x}_m^f - \overline{\boldsymbol{x}}^f \right]. \tag{10b}$$

Note that we have dropped the time subscript k, the subscripts used here refer to individual ensemble members. The forecast error covariance matrices $\mathbf{P}^f$ are then constructed through

$$\mathbf{P}^f = (\mathbf{X}^f)(\mathbf{X}^f)^{\mathrm{T}}. \tag{11}$$

To preserve the variance of the ensemble through the analysis step, square-root (deterministic) schemes for ensemble Kalman filtering are often used. One such scheme is the ensemble transform Kalman filter (ETKF) developed by Bishop et al. (2001) then further adapted for large, spatiotemporally chaotic systems by Hunt et al. (2007). In such schemes, the observations do not need to be perturbed to preserve the analysis covariance in equation (9c). The main idea is that a transform matrix $\mathbf{T}$ can be used to adjust the ensemble analysis anomalies matrix,

$$\mathbf{X}^a \equiv \frac{1}{\sqrt{m-1}} \left[\boldsymbol{x}_1^a - \overline{\boldsymbol{x}}^a, \ldots, \boldsymbol{x}_m^a - \overline{\boldsymbol{x}}^a \right] = \mathbf{X}^f \mathbf{T}, \tag{12}$$

which ultimately forms the analysis error covariance matrix,

$$\mathbf{P}^a = (\mathbf{X}^a)(\mathbf{X}^a)^{\mathrm{T}}. \tag{13}$$

This transform matrix $\mathbf{T}$ is recovered through calculating the ensemble perturbations in normalized observation space,

$$\mathbf{ES} = (\mathbf{R}^{-1/2}\mathbf{H}\mathbf{X}^f)^{\mathrm{T}}(\mathbf{R}^{-1/2}\mathbf{H}\mathbf{X}^f), \tag{14}$$

The transform matrix $\mathbf{T}$ is then defined as

$$\mathbf{T} = (\mathbf{I} + \mathbf{ES}^{\mathrm{T}}\mathbf{ES})^{-1/2}, \tag{15}$$

where $\mathbf{I}$ is the $m \times m$ identity matrix. See Bishop et al. (2001) for the full derivation. This leads to the update of the ensemble mean and the individual ensemble members to their analyzed state through the equations:

$$\overline{\boldsymbol{x}}^a = \overline{\boldsymbol{x}}^f + \mathbf{K}(\boldsymbol{y} - \mathbf{H}\overline{\boldsymbol{x}}^f), \tag{16a}$$

$$\boldsymbol{x}_n^a = \overline{\boldsymbol{x}}^a + (\sqrt{m-1})[\mathbf{X}^f\mathbf{T}]_{*,n}. \tag{16b}$$

~~The~~ Following Bishop et al. (2001) we define the Kalman gain $\mathbf{K}$ ~~is defined~~ through equation (9a), and the ~~notation~~ subscript $*,n$ denotes taking the n-th column of the matrix.

Another deterministic scheme for ensemble Kalman filtering which uses a left-multiplied transform matrix was shown by Tippett et al. (2003) to be equivalent to ETKF:

$$\mathbf{X}^a = \mathbf{T}\mathbf{X}^f, \tag{17a}$$

$$\mathbf{T} = (\mathbf{I} - \mathbf{KH})^{1/2}. \tag{17b}$$

We will refer to this left-multiplied transform filter as the ensemble square-root filter (ESRF). The ensemble mean is updated through (16a) and the individual ensemble members are then updated through:

$$\boldsymbol{x}_n^a = \overline{\boldsymbol{x}}^a + (\sqrt{m-1})[\mathbf{T}\mathbf{X}^f]_{*,n}. \tag{18}$$

When using ensemble Kalman filtering methods like the ones introduced here, sampling errors can often occur. For non-linear models in particular, there is a systematic underestimation of analysis error covariances which eventually leads to filter divergence ~~(Anderson and Anderson, 1999)~~(Anderson and Anderson, 1999; Bocquet et al., 2015; Raanes et al., 2019). This is commonly avoided through the use of inflation. In other words, after each analysis step the ensemble anomalies are inflated through

$$\boldsymbol{x}_n^a = \overline{\boldsymbol{x}}^a + \lambda(\boldsymbol{x}_n^a - \overline{\boldsymbol{x}}^a), \qquad \lambda > 1, \tag{19}$$

where $(\lambda - 1)/100$ is the percentage inflation. Grudzien et al. (2018b) recently showed that the need for inflation tuning could potentially be compensated by including the asymptotic stable modes which produce transient instabilities. The following section introduces one way to account for such transient instabilities through a projection of the forecast error covariance matrix onto a subset of CLVs.

4.2 Ensemble filtering in reduced subspace

Here we define the error covariance matrix $\mathbf{P}^f$ based on the directions of growth and decay of ~~model~~ errors associated with different timescales at the given analysis time. Specifically, we construct $\mathbf{P}^f$ using the ~~local covariant Lyapunov vectors (CLVs)~~ CLVs computed at each data assimilation time step where the number of CLVs is determined by the local attractor dimension $\dim_{KY}$. This allows for the inclusion of unstable, neutral and stable directions dependent on the local dynamics of the system. This differs to past approaches where the subspace was determined in terms of the ~~long time averaged (invariant) unstable and neutral CLVs (Trevisan and Uboldi, 2004; Carrassi et al., 2008; Trevisan and Palatella, 2011)~~asymptotic Lyapunov exponents, and therefore the rank of the error covariance matrix was kept fixed (Trevisan and Uboldi, 2004; Carrassi et al., 2008; Trevisan and Palatella
.

To determine the number of CLVs required to form the basis for $\mathbf{P}^f$, we use the time dependent or local $\dim_{KY}$ rounded up to an integer value. To determine how to weight the individual CLVs, we deconstruct the ensemble anomalies matrix defined in (10b), $\mathbf{X}^f$, into

$$\mathbf{X}^f = \mathbf{\Phi}\mathbf{W}, \tag{20}$$

where $\mathbf{\Phi}$ is a matrix with columns equal to the CLVs (ϕ_i) and $\mathbf{W}$ is a matrix of weights. The columns of $\mathbf{\Phi}$ are ordered according to the corresponding FTLEs in descending order (the first being the direction corresponding to fastest unstable growth). In this formulation $\mathbf{\Phi}$ need not be square, i.e. the CLVs used ~~don't~~ do not need to span the entire space. We compute the CLVs at the assimilation step using Algorithm 1. Equation (20) can then be solved for $\mathbf{W}$ in a least squares sense through

$$\mathbf{W} = (\mathbf{\Phi}^{\mathrm{T}}\mathbf{\Phi})^{-1}\mathbf{\Phi}^{\mathrm{T}}\mathbf{X}^f. \tag{21}$$

The weights in $\mathbf{W}$ combined with the directions in $\mathbf{\Phi}$ now define an object with dimension equal to the chosen number of CLVs whose covariance matrix is defined by

$$\mathbf{P}^f = \mathbf{\Phi}\mathbf{W}\mathbf{W}^{\mathrm{T}}\mathbf{\Phi}^{\mathrm{T}}. \tag{22}$$

We can then use the formulation of $\mathbf{P}^f$ above in conjunction with the ensemble schemes of Section 4.1. We use the modified forecast covariance matrix (22) in the calculation of the Kalman gain (9a) which then also alters any subsequent calculations.

It is important that we span the local dimension of the attractor within the ensemble DA framework in order to avoid ensemble collapse. As mentioned in Section 3, the Kaplan-Yorke dimension computed from the FTLEs is an upper bound to the true local dimension. Figure 7 shows the alignment of the CLVs at two time instances of a model run where the leading FTLEs behave similarly and consequently the Kaplan-Yorke dimensions are approximately the same. In the first case ($t = 306.24$), the leading 5 CLVs are strongly aligned as well as the two most stable (8 and 9). The dimension based on alignment would then intuitively be around 4, and one would need to select the set of CLVs that are not aligned in order to avoid ensemble collapse. According to our method, since the local Kaplan-Yorke dimension is greater than 7 we would retain the leading 8 CLVs, therefore retaining all necessary directions to maintain spread. The second case ($t = 705.04$) shows very different alignment

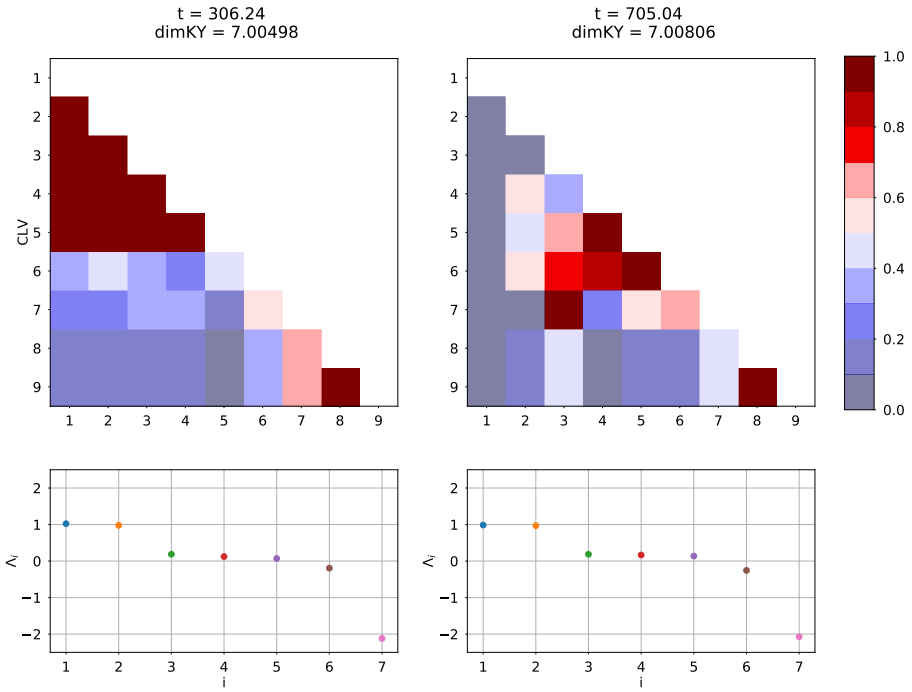

Figure 7. We compare the alignment of the CLVs at two time steps of a model run. The two time steps have similar Kaplan-Yorke measure and distribution of leading FTLEs, shown in the bottom panels. We observe that the behaviour of the alignment can be vastly different for similar FTLE behaviour, however the method of retaining CLVs based on the Kaplan-Yorke measure gives a reliable way to reflect the true local dimension regardless of alignment.

behaviour. Here the leading CLVs are not strongly aligned, but there is strong alignment of CLVs 4-6 and pairs 3,7 and 8,9. This would give an alignment-based dimension around 5, but again we need to retain up to the 8th CLV to span the independent directions. While one could create a method based on alignment for selecting directions, we point out that the actual criteria for "strong alignment" is arbitrary and one could risk excluding a significant direction. For this reason we argue that the local Kaplan-Yorke measure gives a conservative estimate for the number of CLVs to retain.

5 Results

We perform a collection of data assimilation experiments for system (1) using a control run as observations (computed using a Runga-Kutta 4th order scheme with $\Delta t = 0.01$). Here we emphasize that we are interested in exploring the dynamical attributes of data assimilation across multiple timescales. In all cases we are using standard strong CDA, meaning that the cross-covariances are used amongst all components regardless of the observation set (Laloyaux et al., 2016; O'Kane et al., 2019). This allows for the analysis increment of any unobserved subsystems to be influenced by the observations, even in cases of weak coupling between the subsystems. We experiment with different observation sets to explore the applicability and

performance of the variable-rank strong CDA with incomplete or temporally correlated observations. Such observation sets are arguably more realistic representations of the types of observations used in climate applications.

The initialisation settings for the DA experiments are as follows, unless otherwise stated. We use the settings from Yoshida and Kalnay (2018): ~~analysis~~ assimilation window 0.08, inflation factor 1% (optimal for all experiments unless noted otherwise), and 10 ensemble members. We run the model for 75000 time steps (9375 ~~analysis~~ assimilation windows) and use 50000 time steps (6250 ~~analysis~~ assimilation windows) for calculating analysis error statistics. The model is let spin-up for 400 time steps before starting the assimilation cycles as we are using a window of $\tau = 4$ for the calculation of the FTLEs and CLVs. We note that for the CLV method, the system must be sufficiently tracking the control to accurately calculate the initial CLVs. For this reason we start the assimilation before there is significant ensemble divergence. The ensemble members are initialised as perturbations from the control initial condition, taken from a uniform distribution defined on $[-0.025, 0.025]$.

The dynamical properties of the experiments are calculated with respect to the ensemble mean trajectory. The FTLEs are computed using the QR decomposition over the previous 400 time steps leading up to the assimilation time step. The local Kaplan-Yorke dimension is then calculated from the FTLEs. The CLVs are then calculated using a slight modification to Algorithm 1- due to the absence of an accurate future trajectory of the ensemble mean, we do not perform the reorthogonalization to the eigenvectors of $\mathcal{A}(x^{i-n}, N)^* \mathcal{A}(x^{i-n}, N)$ (step 4). This is equivalent to using Algorithm 2.1 of Froyland et al. (2013). We use the previous 400 time steps of the ensemble mean trajectory leading up to the assimilation time step to compute the matrix cocycle and subsequently the CLVs.

5.1 Constructing the observations

In the Kalman filtering method introduced in Section 4, there is an underlying assumption that the observations have some error with variance $\mathbf{R}$. This error variance is typically unknown and chosen *a priori*. If we consider the observations in a statistical sense, we can deconstruct them at each assimilation step into a mean field and perturbation value: $\boldsymbol{y} = \overline{\boldsymbol{y}} + \hat{\boldsymbol{y}}$. In such a formulation, $\overline{\boldsymbol{y}}$ would be the truth at a given point in time and the observation error variance would be the average of the variance of the perturbations, $\mathbf{R} = \overline{\hat{\boldsymbol{y}}\hat{\boldsymbol{y}}^{\mathrm{T}}}$. To emulate this in deterministic models where the truth $\overline{\boldsymbol{y}}$ is known (*i.e.* from a control run), it is common practice to construct the observations by adding to the truth a random value $\hat{\boldsymbol{y}}$ taken from a normal distribution with variance given by the diagonals of $\mathbf{R}$. However, this produces uncorrelated observation errors which have the same variance at any given point in phase space. ~~We argue here that in reality,~~ In many applications the true variance of the observation error can be spatially dependent and errors are often correlated in time (O'Kane and Frederiksen, 2008). We therefore also consider the case where there is error in the observations but it is consistent with the underlying nonlinear dynamics by constructing a trajectory that 'shadows' the truth. Both types of observational errors, with the additional case of perfectly observing a subset of variables, are explored.

The main differences in our subsequent experiments are in the subset of observations used and their corresponding observational errors. We aim to asses the performance of the reduced-rank strong CDA within the different configurations. We first present a benchmark test on the CLV method which is identical to an experiment presented in Yoshida and Kalnay (2018) where the y-component of each subsystem is observed. The perturbations to the control run are from a normal distribution with

error variance $\mathbf{R} = \text{diag}([1, 1, 25])$. This case is referred to as *benchmark observations*. We then consider two experiments where the observations are less sparse within the subsystems, however one subsystem is completely unobserved: *atmosphere observations* (y_e, z_e, y_t, z_t) and *ENSO observations* (y_t, z_t, Y, Z). For the atmosphere observations case we sample the perturbations from error variance $\mathbf{R} = \mathbf{I}_4$, while for the ENSO observations we experiment with different error variances. We then consider correlated observation errors through *shadowed observations*. For these experiments the observation error variances $\mathbf{R}$ are set to the standard values from Yoshida and Kalnay (2018), but the actual perturbations are constructed through a model trajectory which is initialized close to the control run and forced by a relaxation term back to the control. The observation errors then also reflect the local nonlinear growth. We repeat the benchmark, atmosphere, and ENSO observation cases with this type of observation error. Finally, we reduce the observation space to only the extratropical subsystem (x_e, y_e, z_e). This extends upon the work in O'Kane et al. (2019) where the authors considered only ocean observations (X, Y, Z). Due to the difficulty of constraining a system through only fast, weakly coupled dynamics, we decrease the ~~analysis window and do not perturb the control run at all when taking the~~ assimilation window and assume perfect observations.

5.2 Benchmark observations

The first DA experiment we consider is a benchmark case with observations (y_e, y_t, Y). We reproduce the results in Yoshida and Kalnay (2018) using the CLV method introduced in section 4.2. We first perform a DA experiment using a full rank covariance matrix (equivalent to the ETKF method introduced in section 4.1) and then compare to using reduced subspace methods. The first reduced subspace method uses a fixed number of CLVs defined by spanning the asymptotic unstable and neutral subspace plus the first stable mode as in Ng et al. (2011). The second reduced subspace method also uses a fixed number of CLVs, except the number is defined by the asymptotic Kaplan-Yorke dimension as suggested in Carrassi et al. (2008) (note in that study the authors discuss the number of ensemble members which is equivalent to rank of covariance matrix). These fixed numbers are 5 and 6 CLVs, respectively. Finally we analyse our novel reduced subspace method which uses a variable number of CLVs based on the local Kaplan-Yorke dimension. We note that all experiments perform similarly when using the BLVs instead of the CLVs, however BLVs do not provide the same local phase-space information. While we focus on the performance of the CLV method in this work, we include a comparison using BLVs for the experiment utilising local dimension.

The error statistics of all the experiments are listed in Table 2. The analysis RMSE is calculated for each subsystem individually at every ~~analysis window~~ assimilation step and then averaged over the ~~windows~~steps, in line with the error statistics produced in Yoshida and Kalnay (2018). We also calculate the average RMSE of the full system. The RMSE is defined as

$$\text{RMSE} = \sqrt{\frac{1}{N}(\overline{\boldsymbol{x}}^a - \boldsymbol{x})^{\mathrm{T}}(\overline{\boldsymbol{x}}^a - \boldsymbol{x})}, \tag{23}$$

where N is the number of states in the analysed system (either 3 or 9) and $\boldsymbol{x}$ is the truth (control run in our case). ~~Additional metrics calculated for each observed state variable include:~~

$$\text{spread} = \sqrt{\sum_{n=1}^{m} (\boldsymbol{x}_n^f - \overline{\boldsymbol{x}}^f)^2}, \qquad \text{average increment} = \frac{1}{m}\sum_{n=1}^{m} (\boldsymbol{x}_n^a - \boldsymbol{x}_n^f),$$

$$\text{MAD} = \frac{1}{m}\sum_{n=1}^{m} |\boldsymbol{y} - \mathbf{H}\boldsymbol{x}_n^f|, \qquad \text{bias} = \frac{1}{m}\sum_{n=1}^{m} (\boldsymbol{y} - \mathbf{H}\boldsymbol{x}_n^f).$$

We also calculate the spread and average increment for each state variable through

$$\text{spread} = \sqrt{\text{diag}(\mathbf{P}^f)}\,, \qquad \text{average increment} = \overline{(\boldsymbol{x}^a - \boldsymbol{x}^f)}\,. \tag{24}$$

Finally, we calculate the bias with respect to our observations $\boldsymbol{y}$,

$$\text{bias} = \overline{(\boldsymbol{y} - \mathbf{H}\boldsymbol{x}^f)}. \tag{25}$$

Method	Observations [error variance]	⟨RMSE⟩ extratropical	⟨RMSE⟩ tropical	⟨RMSE⟩ ocean	⟨RMSE⟩ full	$\langle \dim_{KY} \rangle$
CLVs - 9 (full rank)	y_e, y_t, Y $[1, 1, 25]$	~~0.3111~~ 0.3142	~~0.1619~~ 0.1598	~~0.4951~~ 0.4948	~~0.4017~~ 0.4027	~~5.9311~~ 5.8928
CLVs - 5 (unstable/neutral subspace + 1)	y_e, y_t, Y $[1, 1, 25]$	~~0.3338~~ 0.3123	~~0.3019~~ 0.1843	~~1.0080~~ 0.5920	~~0.6967~~ 0.4550	~~5.9327~~ 5.8870
CLVs - 6 (global dimension)	y_e, y_t, Y $[1, 1, 25]$	~~0.3256~~ 0.3156	~~0.2002~~ 0.1674	~~0.6623~~ 0.5513	~~0.4958~~ 0.4310	~~5.9317~~ 5.8892
CLVs - variable (local dimension)	y_e, y_t, Y $[1, 1, 25]$	~~0.3196~~ 0.3215	~~0.1881~~ 0.1688	~~0.5963~~ 0.5346	~~0.4573~~ 0.4272	~~5.9279~~ 5.8863
BLVs - variable (local dimension)	y_e, y_t, Y $[1, 1, 25]$	0.3149	0.1658	0.5122	0.4141	5.8895

Table 2. Summary metrics of DA experiments using right-transform matrix (15) and benchmark observations (y_e, y_t, Y). The angle brackets $\langle\cdot\rangle$ denote average over ~~analysis~~ assimilation steps. Compare to results in Yoshida and Kalnay (2018). Parameters: ~~analysis~~ assimilation window 0.08, inflation factor 1%, 10 ensemble members.

We observe that all experiments generally succeed at constraining the full system. The trajectories, spread, increments, and error metrics of the variable CLV experiments are shown in Figure 8; all other experiments behave qualitatively similarly. When comparing the reduced subspace experiments to the full rank case in Table 2, we find that using 5 CLVs (unstable, neutral, and one stable) performs worse than the other CLV experiments~~, and there is more than a 100% increase in the average RMSE of the ocean subsystem compared to full rank~~. While using the asymptotic Kaplan-Yorke dimension (6 CLVs) shows

improvement over 5 CLVs, the most improvement is in the variable CLV (and BLV) case. Although all methods produce a comparable average dimension (last column of Table 2), our experiments show that taking into account local variations in dimension is most effective.

To take a closer inspection of the dynamics during the assimilation, Figure 9 shows ~~some~~ the corresponding dynamical properties of the variable CLV experiment in time. The top panel shows the FTLEs computed from the ensemble mean. The first thing to notice is the correlation of the temporal FTLE variations. The most unstable and most stable modes have the same frequency of variability and remain highly correlated throughout the whole experiment. The lower frequency variations seen in the second most stable mode are often correlated with some of the weakly stable modes. These seem to have the biggest impact on the local dimension (shown in panel b). We can compare the changes in FTLEs and local dimension to the rank of the covariance matrix (panel c). A decrease in local dimension typically occurs when one of the weakly stable modes becomes more stable, and therefore less CLVs are needed to span the local unstable and neutral subspace. On the contrary, when the dimension increases the weakly stable modes have become more unstable, at times even becoming positive. This implies that more CLVs are needed to span the local unstable and neutral subspace, and therefore the rank of the covariance matrix increases. The local Kolmogorov-Sinai entropy is also shown with the local dimension. We see that directly before a full dimension collapse ($\dim_{KY} = 0$), there is a spike in local entropy. A collapse in dimension here occurs when all the FTLEs become negative. This does not impact the effectiveness of the method, however, as it just enforces the covariance matrix and Kalman gain to be zero for that analysis step. The ensemble members are not adjusted and therefore left to evolve accordingly. The bottom panel of Figure 9 shows the statistics of the FTLEs. The mean values, shown as a full circle, are used to calculate the average dimension in Table 2. These can be compared to the asymptotic values computed in Section 2.2 which are shown as open circles to the right of the FTLE statistics. We also show the standard deviation for each of the FTLEs. The largest standard deviations are found in the fifth and sixth FTLEs, which correspond to the first two stable modes of the system. This supports the hypothesis that the weakly stable modes are most influential in the variation of local dimension. We also see that the maximum values ~~(squares)~~ are greater than (or equal to) zero. This implies that at a given time the fifth and sixth modes have moved into the unstable/neutral subspace and additional modes are therefore needed to account for nonlinear error growth.

5.3 Atmosphere observations

We now consider the case where only the two atmosphere subsystems are observed, however the observations are less sparse within each subsystem in that we take both the y and z components~~from each subsystem~~. Yoshida and Kalnay (2018) considered a similar case ~~with~~ where only y component observations were used with the cross-covariances in the atmosphere, but the ocean was also observed and assimilated separately. Here we rely only on the cross-covariances to recover the ocean subsystem, as the ocean is strongly coupled to the tropical atmosphere. For this case we use the following settings: ~~analysis~~ assimilation window 0.08, observation error covariance matrix $\mathbf{R} = I_4$, inflation factor 1%, and 10 ensemble members. The model is run for the same amount of time as in the benchmark observations experiments.

Table 3 shows the summary statistics of performing full rank DA (9 CLVs), rank equal to the number of CLVs corresponding to asymptotic dimension, and a variable rank equal to number of CLVs corresponding to local dimension. ~~In such~~

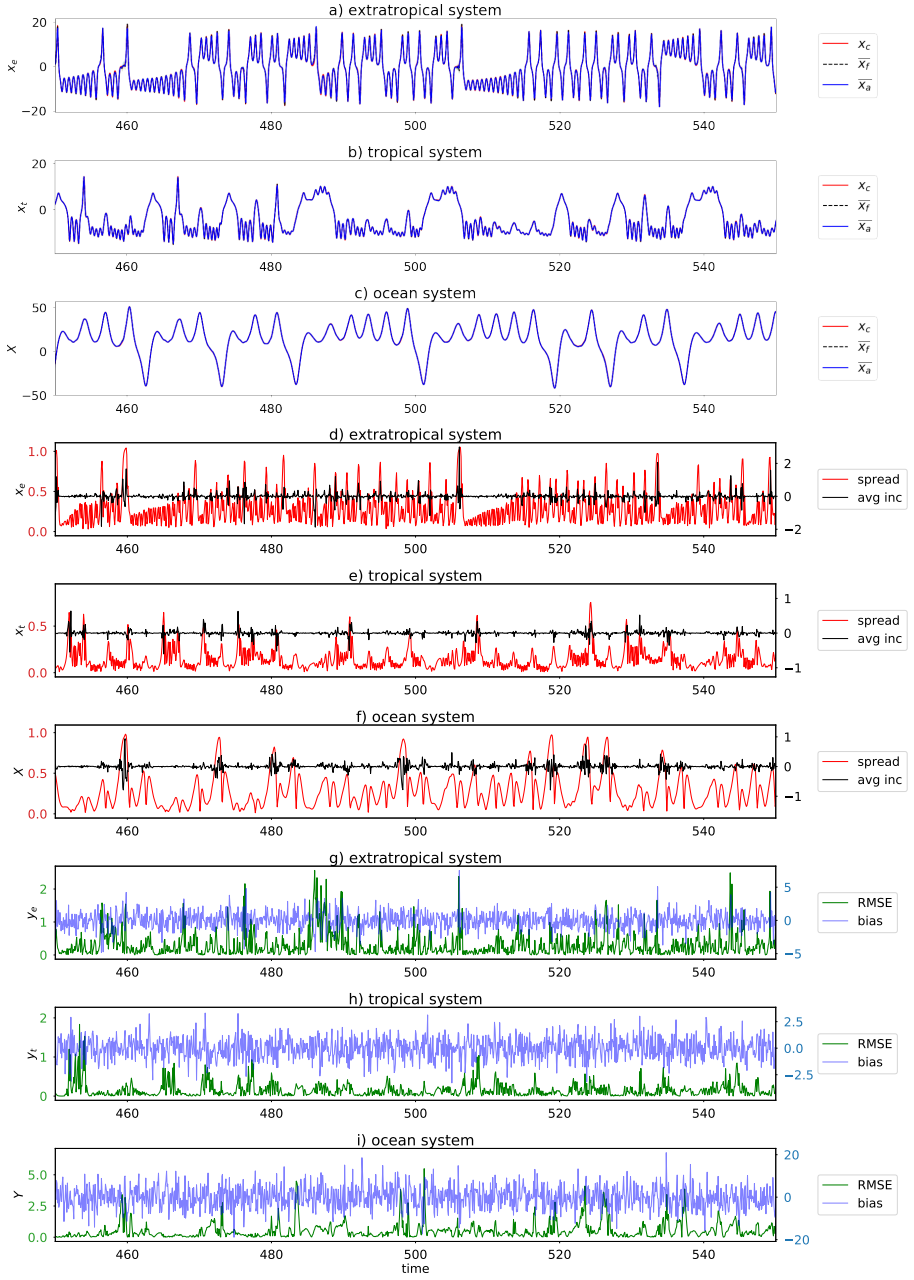

Figure 8. Segment of DA using the variable CLV method and benchmark observations (y_e, y_t, Y). (a-c) Trajectories shown are control run (red), ensemble mean (blue), and individual ensemble members (faint). (d-f) Metrics shown are size of ensemble spread (red) and ensemble mean increment (black). (g-i) Metrics shown are root mean ~~absolute deviation~~ square error (~~MAD~~RMSE, ~~red~~green) and bias (blue). For conciseness we only show the results for one coordinate of each subsystem. The other two coordinates behave similarly. Parameters: ~~analysis~~ assimilation window 0.08, inflation factor 1%, 10 ensemble members, observation error covariance matrix $\mathbf{R} = \mathrm{diag}([1, 1, 25])$.

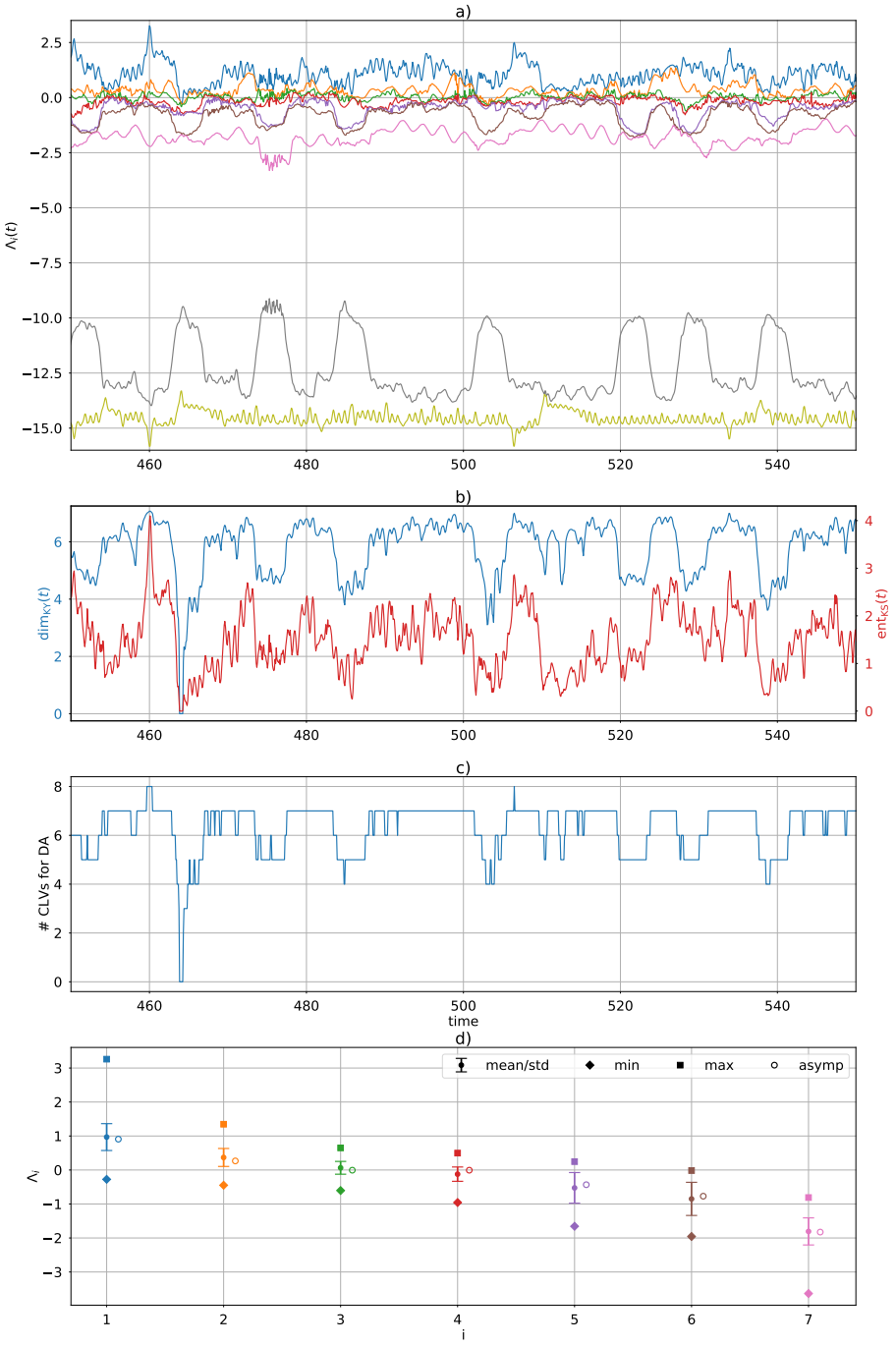

Figure 9. Local attractor properties of DA using the variable CLV method and benchmark observations (y_e, y_t, Y). (a) FTLEs calculated from the ensemble mean trajectory over a window of $\tau = 4$. (b) Local Kaplan-Yorke dimension and Kolmogorov-Sinai entropy computed through (2) and (3) using the FTLEs at the given time. (c) Rank of covariance matrix. (d) Statistics of first 7 FTLEs compared to asymptotic values.

Method	Observations [error variance]	⟨RMSE⟩ extratropical	⟨RMSE⟩ tropical	⟨RMSE⟩ ocean	⟨RMSE⟩ full	$\langle \dim_{KY} \rangle$
CLVs - 9	y_e, z_e, y_t, z_t $[1,1,1,1]$	~~0.1757~~ 0.1734	~~0.1392~~ 0.1332	~~0.5892~~ 0.5782	~~0.4598~~ 0.4515	~~5.9134~~ 5.8672
CLVs - 6	y_e, z_e, y_t, z_t $[1,1,1,1]$	~~0.6656~~ 0.1715	~~3.5193~~ 0.1386	~~18.7334~~ 0.5807	~~12.8749~~ 0.4524	~~5.8591~~ 5.8718
CLVs - variable	y_e, z_e, y_t, z_t $[1,1,1,1]$	~~0.1890~~ 0.1697	~~0.1804~~ 0.1383	~~0.8146~~ 0.5659	~~0.6062~~ 0.4433	~~5.9152~~ 5.8681

Table 3. Summary metrics of DA experiments using right-transform matrix (15) and atmosphere observations (y_e, z_e, y_t, z_t). Parameters: ~~analysis~~ assimilation window 0.08, inflation factor 1%, 10 ensemble members.

~~a case where we rely only on observations from the fast timescale subsystems, the asymptotic dimension is insufficient for tracking the system. When using a set number of 6 CLVs the tropical atmosphere and ocean subsystems begin following a different trajectory than the control run (Figure **??**). This eventually also leads to the extratropical subsystem following a different trajectory ($t \approx 730$). On the other hand, the variable CLV method has no difficulty in tracking the control run for all the subsystems, and it has summary statistics comparable to the full rank experiment (Figure **??** and~~ All experiments have comparable summary statistics, however the variable CLV experiment slightly out-performs both fixed-rank methods (Table 3).

~~Trajectories of DA using 6 CLVs (a-c) and variable CLVs (d-f) with atmosphere observations (y_e, z_e, y_t, z_t). Trajectories shown are control run (red), ensemble mean (blue), and individual ensemble members (faint). For conciseness we only show the results for the x-coordinate of each subsystem. The other two coordinates behave similarly. Parameters: analysis window 0.08, inflation factor 1%, 10 ensemble members, observation error covariance matrix $\mathbf{R} = I_4$.~~

~~We again analyse~~ We also analysed the dynamical properties of the variable CLV experiment ~~to understand why the 6 CLV method fails to track the control run. The FTLEs, local Kaplan-Yorke dimension, local Kolmogorov-Sinai entropy, number of CLVs, and FTLE statistics are shown in Figure **??**. We see that just before the tropical and ocean subsystems first fail to track the control run in the 6 CLV experiment ($t \approx 465$), there is a spike in the local Kolmogorov-Sinai entropy and the number of CLVs increases to 8. There are other instances where the local Kaplan-Yorke dimension calls for 8 CLVs, however the combination of the spike in entropy and dimension seems to be the driving factor behind the 6 CLV method failing. Note that this is unique to the case where one subsystem is unobserved and assimilated solely based on cross-covariances. There is also a spike in local entropy and dimension in the benchmark observations case~~ and did not find any significant differences to those of the benchmark experiment (Figure 9)~~, however the 6 CLV method succeeds in tracking the control run when all the subsystems are partially observed. The statistics of the FTLEs are similar to those of the benchmark case, except the maximum value of the sixth FTLE is clearly larger and the minimum value of the first FTLE is no longer negative (hence the absence of total dimension collapse).~~ .

~~Local attractor properties of DA using variable CLVs and atmosphere observations (y_e, z_e, y_t, z_t). (a) FTLEs calculated from the ensemble mean trajectory over a window of $\tau = 4$. (b) Local Kaplan-Yorke dimension and Kolmogorov-Sinai entropy computed through (2) and (3) using the FTLEs at the given time. (c) Rank of covariance matrix. (d) Statistics of first 7 FTLEs compared to asymptotic values.~~

5.4 ENSO observations

The strong coupling and low frequency variation in the ocean and tropical atmosphere subsystems represent an ENSO-like variability. We therefore refer to the case of observing the y and z components from the tropical and ocean subsystems as ENSO observations. Again, this is similar to a case studied in Yoshida and Kalnay (2018) except we don't assimilate the extratropical atmosphere at all and attempt to recover the variability solely through the cross-covariances. We don't expect to track the control trajectory of the extratropical system, but we are interested to see if we can ~~preserve the variance of~~ avoid collapse (*i.e.* the loss of variability) in the ensemble mean ~~for~~ of the extratropical attractor.

Since the extratropical subsystem is likely to be unconstrained with these observations, the ensemble mean will not be accurately estimated. In such a case, the variable CLV method fails due to the fact that the first CLV (which corresponds to the directions of fastest error growth) is inaccurately calculated. Therefore the true directions of unstable growth are inaccurately sampled in the reduced space experiments. This is amplified by the fact that we are using uncorrelated observation errors; if the observation errors have a temporal correlation, the dominant direction of nonlinear unstable growth can be ascertained even without tracking the extratropical subsystem (see following section on shadowed observations). The inaccurate dimension reduction leads to exponential growth in the system and numerical instability. For this reason we turn our focus only on the full rank (9 CLV) method and the accuracy of the observations.

We use the following settings for all the DA experiments with ENSO observations: ~~analysis~~ assimilation window 0.08, inflation factor 1%, and 10 ensemble members. The model is run for the same amount of time as in the benchmark observations experiments. We study the effect of reducing the observation error variances in $\mathbf{R}$: standard observation error ($\mathbf{R} = \mathrm{diag}([1, 1, 25, 25])$), reduced tropical atmosphere error ($\mathbf{R} = \mathrm{diag}([0.01, 0.01, 25, 25])$), reduced ocean error ($\mathbf{R} = \mathrm{diag}([1, 1, 0.25, 0.25])$), and reduced overall error ($\mathbf{R} = \mathrm{diag}([0.01, 0.01, 0.25, 0.25])$). The summary statistics are listed in Table 4 for all the experiments.

We find that for the standard observation errors, there is a collapse in the variance of the ensemble mean for the extratropical subsystem (Figure 10). However, when the observation error for the tropical subsystem is reduced, that variance is significantly increased. This can be seen through the increase in the average local Kaplan-Yorke dimension (Table 4). There is also a slight increase in the ability to track the extratropical subsystem of the control run. We note that decreasing the ocean observation error alone does not provide any improvements over the total error statistics or dimension, actually making them slightly worse. When the observation error of both subsystems is reduced, there is only a small improvement to the overall error statistics and dimension in comparison to the reduced tropical error case. The improvement is most notable for the cases with reduced tropical observation errors due to the tropical system's weak direct coupling to the extratropical system.

Method	Observations [error variance]	⟨RMSE⟩ extratropical	⟨RMSE⟩ tropical	⟨RMSE⟩ ocean	⟨RMSE⟩ full	$\langle \dim_{KY} \rangle$
CLVs - 9	y_t, z_t, Y, Z $[1, 1, 25, 25]$	~~6.9336~~ 7.0467	~~0.1488~~ 0.1571	~~0.3626~~ 0.3675	~~4.6428~~ 4.7182	~~4.5416~~ 4.5449
CLVs - 9	y_t, z_t, Y, Z $[0.01, 0.01, 25, 25]$	~~5.5029~~ 5.5203	~~0.0479~~ 0.0480	~~0.1742~~ 0.1764	~~3.6743~~ 3.6860	~~5.4347~~ 5.4052
CLVs - 9	y_t, z_t, Y, Z $[1, 1, 0.25, 0.25]$	~~7.0781~~ 7.1308	~~0.1277~~ 0.1386	~~0.0838~~ 0.0873	~~4.7212~~ 4.7566	~~4.6362~~ 4.4959
CLVs - 9	y_t, z_t, Y, Z $[0.01, 0.01, 0.25, 0.25]$	~~5.1399~~ 5.1697	~~0.0457~~ 0.0431	~~0.0901~~ 0.0822	~~3.4286~~ 3.42478	~~5.4480~~ 5.4899

Table 4. Summary metrics of DA experiments using right-transform matrix (15) and ENSO observations (y_t, z_t, Y, Z). Parameters: ~~analysis~~ assimilation window 0.08, inflation factor 1%, 10 ensemble members.

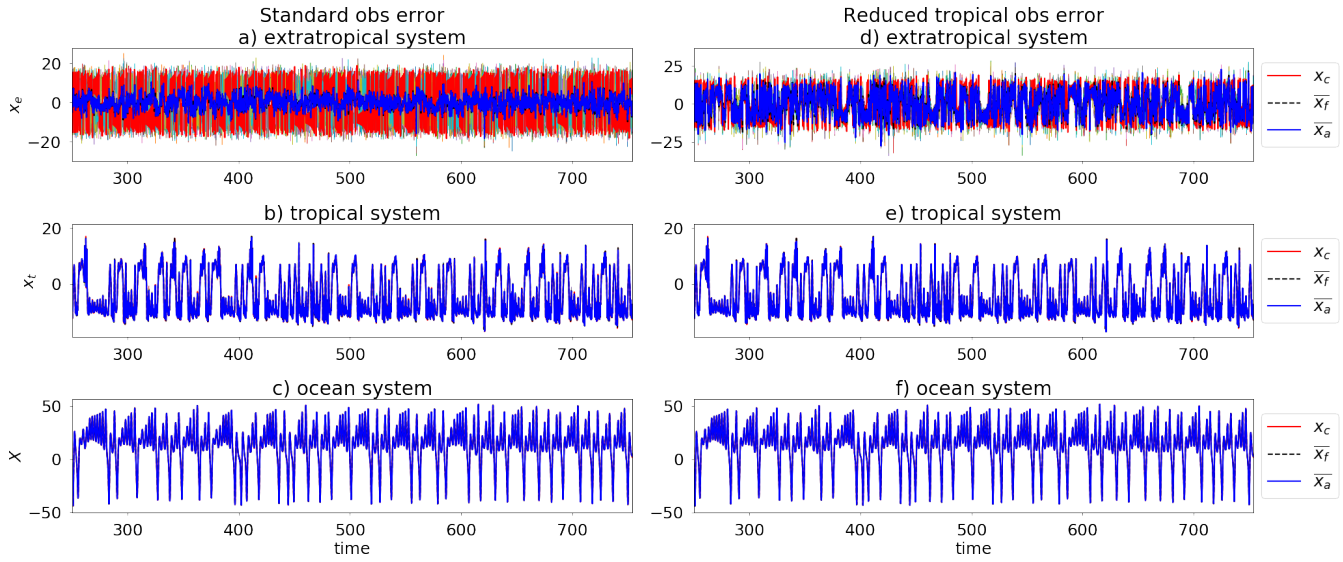

Figure 10. Trajectories of DA using 9 CLVs, $\mathbf{R} = \mathrm{diag}([1, 1, 25, 25])$ (a-c) and $\mathbf{R} = \mathrm{diag}([0.01, 0.01, 25, 25])$ (d-f) with ENSO observations (y_t, z_t, Y, Z). Trajectories shown are control run (red), ensemble mean (blue), and individual ensemble members (~~faint~~multicoloured). For conciseness we only show the results for the x-coordinate of each subsystem. The other two coordinates behave similarly. Parameters: ~~analysis~~ assimilation window 0.08, inflation factor 1%, 10 ensemble members.

5.5 Shadowed observations

In this section we explore a different type of observation error. Rather than randomly perturbing the control run to form our observation points, we use a trajectory that shadows the control run which produces correlated observational errors. In other

words, we construct a new trajectory with a relaxation to the control run. This is implemented into the model as follows:

$$\dot{\tilde{x}}_e = \sigma(\tilde{y}_e - \tilde{x}_e) - c_e(S\tilde{x}_t + k_1), \tag{26a}$$

$$\dot{\tilde{y}}_e = \rho\tilde{x}_e - \tilde{y}_e - \tilde{x}_e\tilde{z}_e + c_e(S\tilde{y}_t + k_1) + \alpha_1(y_e - \tilde{y}_e), \tag{26b}$$

$$\dot{\tilde{z}}_e = \tilde{x}_e\tilde{y}_e - \beta\tilde{z}_e, \tag{26c}$$

$$\dot{\tilde{x}}_t = \sigma(\tilde{y}_t - \tilde{x}_t) - c(S\tilde{X} + k_2) - c_e(S\tilde{x}_e + k_1), \tag{26d}$$

$$\dot{\tilde{y}}_t = \rho\tilde{x}_t - \tilde{y}_t - \tilde{x}_t\tilde{z}_t + c(S\tilde{Y} + k_2) + c_e(S\tilde{y}_e + k_1) + \alpha_2(y_t - \tilde{y}_t), \tag{26e}$$

$$\dot{\tilde{z}}_t = \tilde{x}_t\tilde{y}_t - \beta\tilde{z}_t + c_z\tilde{Z}, \tag{26f}$$

$$\dot{\tilde{X}} = \tau\sigma(\tilde{Y} - \tilde{X}) - c(\tilde{x}_t + k_2), \tag{26g}$$

$$\dot{\tilde{Y}} = \tau\rho\tilde{X} - \tau\tilde{Y} - \tau S\tilde{X}\tilde{Z} + c(\tilde{y}_t + k_2) + \alpha_3(Y - \tilde{Y}), \tag{26h}$$

$$\dot{\tilde{Z}} = \tau S\tilde{X}\tilde{Y} - \tau\beta\tilde{Z} - c_z\tilde{z}_t. \tag{26i}$$

It is sufficient to constrain the trajectory using the relaxation term only in the y-coordinates. The parameters $\alpha_1 = 2.75$, $\alpha_2 = 0.8$, and $\alpha_3 = 0.8$ are the relaxation strengths and $y_e(t)$, $y_t(t)$, and $Y(t)$ are taken from the control trajectory at the given time.

We initialize the shadowed trajectory with a small perturbation to the control trajectory initial condition. We then propagate the shadowed trajectory along with the control trajectory, taking the observations from the shadowed trajectory at each assimilation cycle. Figure 11 shows the difference between the observations constructed using random perturbations and those from the shadowed trajectory. One benefit of the shadowed trajectory which is clearly visible in these figures is that it much more closely maintains the structure of the attractor. This is not the case when using randomized perturbations, where the structure is not as discernible.

We repeat the observation experiments of the previous three sections: benchmark observations, atmospheric observations, and ENSO observations. We only focus on the full rank and variable CLV methods. When using correlated observational errors in any ensemble Kalman filtering method, a larger inflation value and ensemble size are needed to avoid ensemble collapse. We find that for the standard ETKF method increasing the ensemble size to 11 members is sufficient. To facilitate a direct comparison, we therefore also use this ensemble size for the CLV experiments. The inflation value varies slightly with the different observation cases. The setup and results of the experiments are shown in Table 5.

When using the benchmark observation set from the shadowed trajectory, the ~~full rank and variable CLV methods perform comparably~~variable CLV method outperforms the full rank method. This shows improvement over the case with random observation errors discussed in Section 5.2 where the variable CLV method performed slightly worse than the full rank. For the atmosphere observation case, we ~~observe an improvement~~ again observe similar performance when using the variable CLV method ~~over~~ and the full rank, with the largest reduction of average RMSE in the ~~extratropical~~ ocean subsystem. The ~~overall improvement is in contrast to the results when using random observation errors in Section 5.3; in those cases the~~

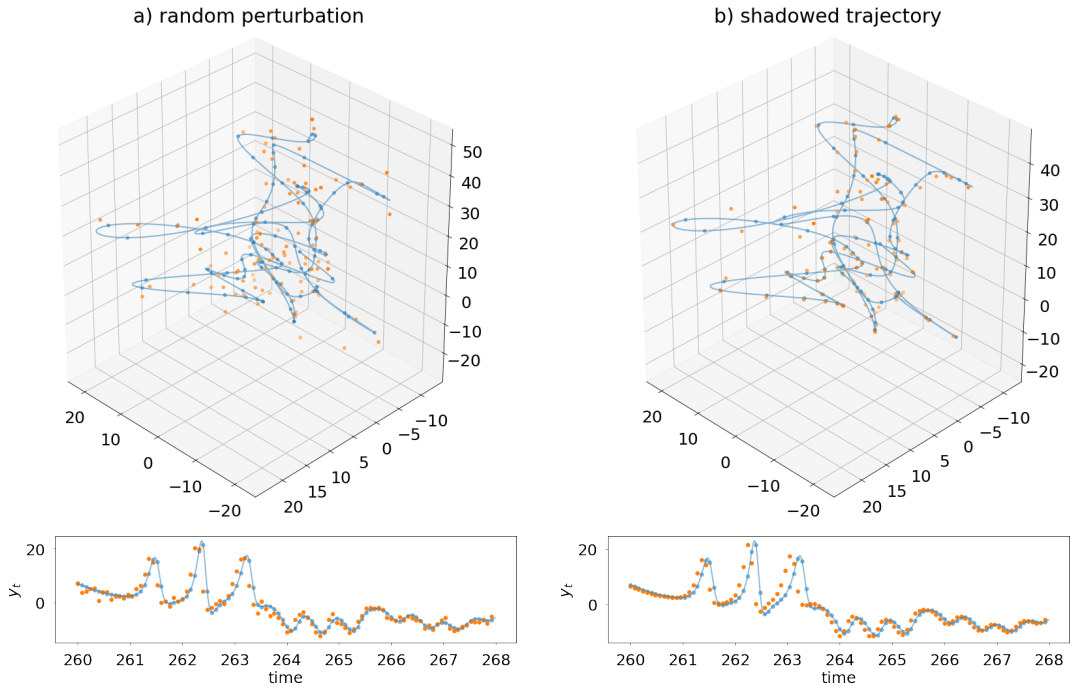

Figure 11. Comparison of the two different types of observations used in the data assimilation experiments. We show the observation space for the benchmark observations case (y_e, y_t, Y). A selection of 800 time steps (100 observations) of the control model (blue line) and values at the observation times (blue dots) are shown in both plots, along with the actual observations used (orange dots). Top figures show behaviour along attractor and bottom panels show y_t in time. (a) Observations formed by random perturbations to control run points. (b) Observations taken from a trajectory which shadows the control run.

~~full rank method outperformed the variable CLV method. The~~ major change in the ENSO observation case from the random observational error experiments in Section 5.4 is that when using the shadowed trajectory observations the variable CLV method no longer fails. There is still difficulty in accurately calculating the first CLV from the extratropical subsystem being unconstrained, however the correlation in the errors of the tropical and ocean subsystems provide additional information about the underlying nonlinear error growth. We observe that the variable CLV method performs comparably to the full rank, with a slightly larger average RMSE in the ocean subsystem (and subsequently the full). The inability to track the extratropical subsystem can once again be seen through the decrease in average local dimension.

5.6 Extratropical observations

We finally consider the case where one subsystem is fully observed and the others are completely unobserved. We choose to observe the extratropical subsystem, as it is the most extreme case with weakly coupled fast dynamics. Due to the difficulty of constraining the full system with such minimal observations, the assimilation window is reduced to 0.02 and we use *perfect*

Method	Observations [error variance]	⟨RMSE⟩ extratropical	⟨RMSE⟩ tropical	⟨RMSE⟩ ocean	⟨RMSE⟩ full	$\langle \dim_{KY} \rangle$
CLVs - 9 3% inflation	$\tilde{y}_e, \tilde{y}_t, \tilde{Y}$ $[1, 1, 25]$	~~0.4825~~ 0.5200	~~0.1604~~ 0.1635	~~0.4303~~ 0.4255	~~0.4361~~ 0.4552	~~5.9566~~ 5.9576
CLVs - variable 3% inflation	$\tilde{y}_e, \tilde{y}_t, \tilde{Y}$ $[1, 1, 25]$	~~0.4926~~ 0.4848	~~0.1630~~ 0.1568	~~0.4158~~ 0.4095	~~0.4335~~ 0.4263	~~5.9722~~ 5.9371
CLVs - 9 ~~4~~3% inflation	$\tilde{y}_e, \tilde{z}_e, \tilde{y}_t, \tilde{z}_t$ $[1, 1, 1, 1]$	~~0.4215~~ 0.4258	~~0.1368~~ 0.1342	~~0.4648~~ 0.4300	~~0.4834~~ 0.4687	~~5.9602~~ 5.9237
CLVs - variable ~~4~~3% inflation	$\tilde{y}_e, \tilde{z}_e, \tilde{y}_t, \tilde{z}_t$ $[1, 1, 1, 1]$	~~0.3773~~ 0.4337	~~0.1366~~ 0.1373	~~0.4663~~ 0.4027	~~0.4653~~ 0.4649	~~5.9582~~ 5.9191
CLVs - 9 4% inflation	$\tilde{y}_t, \tilde{z}_t, \tilde{Y}, \tilde{Z}$ $[1, 1, 25, 25]$	~~6.8620~~ 6.8613	~~0.1440~~ 0.1431	~~0.3067~~ 0.3025	~~4.5962~~ 4.5961	~~4.6264~~ 4.5309
CLVs - variable 4% inflation	$\tilde{y}_t, \tilde{z}_t, \tilde{Y}, \tilde{Z}$ $[1, 1, 25, 25]$	~~6.9726~~ 6.8722	~~0.1404~~ 0.1463	~~0.5528~~ 0.3370	~~4.7305~~ 4.6054	~~4.4854~~ 4.5541

Table 5. Summary metrics of DA experiments using right-transform matrix (15) and shadowed trajectory as observations. We set the observation error covariances to the standard values as in Yoshida and Kalnay (2018). Parameters: ~~analysis~~ assimilation window 0.08, 11 ensemble members, inflation as noted in table.

observations. In other words, we do not add any perturbations to the control run when taking the observation. Having more accurate observations was shown in Section 5.4 to improve the performance of the unobserved subsystems in the assimilation.

It is also clear from the previous experiments that the inability to constrain unobserved subsystems leads to a collapse in dimension, and correspondingly a collapse in the covariances. A collapse in covariance is commonly avoided through the use of inflation (Anderson and Anderson, 1999; Hamill et al., 2001; Carrassi et al., 2008; Raanes et al., 2019). While a static background inflation avoids full covariance collapse, we are interested here in the covariance collapse related only to specific subsystems which aren't being constrained. For such a case, we argue that the forecast error covariance matrix should be scaled by a factor relating to the ensemble performance at each analysis step. In other words, when an individual subsystem is not being constrained, the covariances should be increased in the calculation of the Kalman gain, analogous to the approach outlined by Miller et al. (1994) for the strongly nonlinear Lorenz '63 system. In their study the authors find that the forecast error covariance is often underestimated in such highly nonlinear systems, particularly when the model is in a region of phase space subject to transitions. Subsequently, the Kalman gain is underestimated. The authors account for this by including the third and fourth moments of anomalies in the Kalman gain calculation.

Here we introduce a new method for adaptive scaling of the Kalman gain. ~~At each analysis step we multiply the forecast error covariance matrix by~~ Rather than explicitly calculating higher moments of the anomalies, we account for the underestimation through a spread-dependent ~~scalar factor~~ factor which balances our forecast error covariance $\mathbf{P}^f$ and observation error variance $\mathbf{R}$ accordingly. The idea being that larger spread implies we have underestimated the covariances, and vice versa. We note that

this adaptive scaling is different to traditional inflation as it does not directly adjust the underlying ensemble spread. We use this in conjunction with the static background inflation of 1% to avoid total ensemble collapse.

We scale the ~~error covariance matrix $\mathbf{P}^f$ by the~~ Kalman gain in the following way:

$$\hat{\mathbf{K}} = \frac{||\mathbf{P}^f||\mathbf{P}^f\mathbf{H}^{\mathrm{T}}}{||\mathbf{P}^f||\mathbf{H}\mathbf{P}^f\mathbf{H}^{\mathrm{T}} + \mathbf{R}}, \tag{27}$$

or equivalently

$$\hat{\mathbf{K}} = \mathbf{P}^f\mathbf{H}^{\mathrm{T}}\left[\mathbf{H}\mathbf{P}^f\mathbf{H}^{\mathrm{T}} + \frac{\mathbf{R}}{||\mathbf{P}^f||}\right]^{-1}. \tag{28}$$

Here the scaling factor is the Frobenius norm of ~~$(\mathbf{X}^f)(\mathbf{X}^f)^{\mathrm{T}}$~~$\mathbf{P}^f = (\mathbf{X}^f)(\mathbf{X}^f)^{\mathrm{T}}$, where $\mathbf{X}^f$ is the ensemble spread matrix defined by (10b). This ~~leads to a new scaled error covariance matrix $\hat{\mathbf{P}}^f$ defined by~~

~~$$\hat{\mathbf{P}}^f = ||(\mathbf{X}^f)(\mathbf{X}^f)^{\mathrm{T}}||(\mathbf{X}^f)(\mathbf{X}^f)^{\mathrm{T}},$$~~

~~in the standard ESRF method or~~

~~$$\hat{\mathbf{P}}^f = ||(\mathbf{X}^f)(\mathbf{X}^f)^{\mathrm{T}}||(\mathbf{\Phi}\mathbf{W}\mathbf{W}^{\mathrm{T}}\mathbf{\Phi}^{\mathrm{T}}),$$~~

~~when using the CLVs. This~~ rescaling factor is mathematically similar to the K-factor adaptive quality control procedure introduced by Sakov and Sandery (2017) and the β-factor rescaling of the background error covariances introduced by Bowler et al. (2013). The K-factor method was used to account for inconsistencies in observations and therefore uses an adaptive observation error covariance $\mathbf{R}$ that takes into account innovation size at each analysis step, while the β-factor is a ~~constant multiplier~~ deflation to the forecast error covariance matrix to avoid the underestimation of the ensemble spread ($0 < \beta < 1$). Both the K-factor procedure and the β-factor multiplier can be shown to have the same scaling effect on the Kalman gain $\mathbf{K}$ defined by (9a) as the adaptive scaling presented here, with the difference in that the modified ~~$\hat{\mathbf{P}}^f$ in (??~~$\hat{\mathbf{K}}$ in (28) takes into account both effects: small $||(\mathbf{X}^f)(\mathbf{X}^f)^{\mathrm{T}}||$ behaves like the β-factor and large $||(\mathbf{X}^f)(\mathbf{X}^f)^{\mathrm{T}}||$ behaves like the K-factor. We discuss the limiting behaviour of this adaptive scaling method in terms of the increment size and analysis error covariance in Appendix A.

Due to the fact that only the Kalman gain is being adjusted, for ease of implementation we use ESRF method introduced in Section 4.1. This allows for the left-transform matrix to be calculated with the modified Kalman gain,

~~$$\hat{\mathbf{K}} = \hat{\mathbf{P}}^f\mathbf{H}^{\mathrm{T}}[\mathbf{H}\hat{\mathbf{P}}^f\mathbf{H}^{\mathrm{T}} + \mathbf{R}]^{-1},$$~~

~~$$\mathbf{T} = (\mathbf{I} - \hat{\mathbf{K}}\mathbf{H})^{1/2}.$$~~

$$\mathbf{T} = (\mathbf{I} - \hat{\mathbf{K}}\mathbf{H})^{1/2}. \tag{29}$$

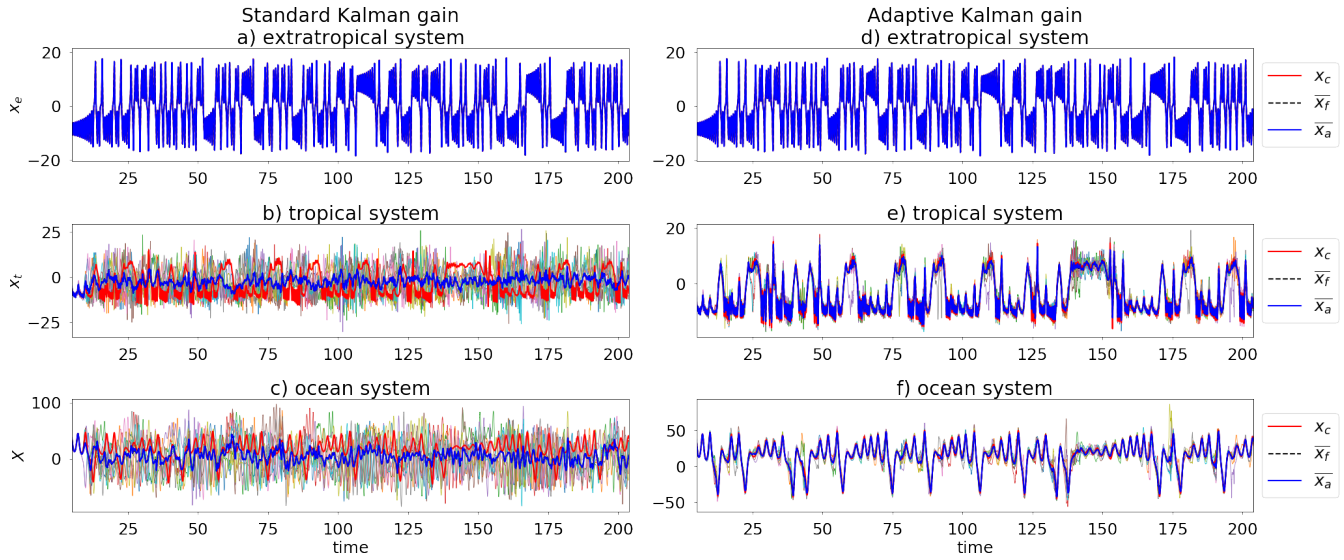

Figure 12. Trajectories of DA experiments using ~~9~~ variable CLVs, left-transform matrix (17b), and perfect observations from the extratropical subsystem of a control run (x_e, y_e, z_e), with (a-c) the standard Kalman gain (9a) and (d-f) the adaptive Kalman gain (28). Trajectories shown are control run (red), ensemble mean (blue), and individual ensemble members (~~faint~~multicoloured). For conciseness we only show the results for the x-coordinate of each subsystem. The other two coordinates behave similarly. Parameters: ~~analysis~~ assimilation window 0.02, inflation factor 1%, 10 ensemble members, observations error covariance $\mathbf{R} = I_4$.

~~We also note that the variable CLV method will be less effective than using the full rank CLV matrix (or equivalent standard ESRF). The reduction in dimension is related to the unobserved subsystems being unconstrained. By using the variable CLV method, we are *a priori* setting the rank of the ensemble member matrix and covariance matrix. This can also have the effect of reducing some cross-covariances further, and thus the scaling implemented here may be ineffective. Therefore, in both methods we use~~ We apply the adaptive gain to both the full rank (9 CLV) and variable rank formulation of the covariance matrix. The results of ~~both experiments , perfect observations and perfect observations with adaptive gain,~~ the variable rank experiments with and without adaptive gain are shown in Figure 12 and the error statistics of all four experiments are listed in Table 6.

We see from Figure 12 that there is a remarkable improvement when using the adaptive gain method. Not only is the ensemble spread reduced in the unobserved subsystems, but the ensemble mean is also able to track the control run. This improvement in tracking the control run is exemplified in Table 6 with significant reduction in the average RMSE of individual subsystems. As expected, the average dimension is also significantly increased.

6 Concluding remarks

This study presents an initial understanding of the transient dynamics associated with the Kalman filter forecast error covariance matrix for nonlinear multiscale coupled systems. We have ~~demonstrated~~ explored the varying rank of the error covariance

Method	Observations [error variance]	⟨RMSE⟩ extratropical	⟨RMSE⟩ tropical	⟨RMSE⟩ ocean	⟨RMSE⟩ full	$\langle \dim_{KY} \rangle$
CLVs - 9	x_e, y_e, z_e [1, 1, 1]	~~0.0666~~ 0.0640	~~8.9288~~ 8.4752	~~38.5408~~ 36.3662	~~22.9953~~ 21.7108	~~4.1240~~ 4.1332
CLVs - var	x_e, y_e, z_e [1, 1, 1]	0.0670	9.4872	40.4894	24.1528	4.1152
CLVs - 9 adaptive gain	x_e, y_e, z_e [1, 1, 1]	0.0032	0.7241	3.5757	2.1504	5.9991
CLVs - var adaptive gain	x_e, y_e, z_e [1, 1, 1]	0.0034	~~0.7648~~ 0.8350	~~3.7789~~ 4.0632	~~2.2671~~ 2.4501	~~6.0229~~ 5.8888

Table 6. Summary metrics of DA experiments using left-transform matrix (17b) and the full extratropical subsystem as observations (x_e, y_e, z_e). We use perfect observations (no random error added to the control run) with the observation error covariances set to the standard values as in Yoshida and Kalnay (2018). Parameters: ~~analysis~~ assimilation window 0.02, inflation factor 1%, 10 ensemble members.

matrix related to the transient growth in the stable modes of the system, and in particular the applicability of this varying rank on different configurations of strong CDA. Additionally, we have shown the large impact of using isolated observations and cross-domain covariances in such a coupled system. The cross-covariances are significantly underestimated when the observed subsystems are weakly coupled to the unobserved, however this can be compensated through either reduced observational error or the use of an adaptive scaling of the Kalman gain.

The dynamical properties of strongly coupled DA in a multiscale system were investigated through a low-dimensional nonlinear chaotic model to represent the interactions between the extratropical atmosphere, ocean, and tropical atmosphere-ocean interface. The model contains significant spatio-temporal scale separations between the subsystems, as well as varying coupling strengths. We introduced a local dimension measure, namely the Kaplan-Yorke dimension calculated using FTLEs, to ~~determine the~~ specify the appropriate rank of the forecast error covariance matrix at each analysis step. We have shown that through using time-varying CLVs to form a reduced rank forecast error covariance matrix, ~~you achieve~~ comparable results to the full rank ETKF and ESRF schemes are achievable.

We considered a benchmark experiment previously explored in Yoshida and Kalnay (2018) to examine the most effective number of CLVs needed to form the forecast error covariance matrix. We found that when using less than full rank, the variable amount based on local dimension performed the best. We also found there was not significant improvement when increasing to full rank. In particular, we found that spanning the space comprised of the asymptotic unstable, neutral, and first weakly stable mode (5 CLVs in this case) performed ~~much~~ worse than using either dimension measure (asymptotic and local). This suggests that significant growth occurring in more than one weakly stable mode is important when capturing short-term dynamics of highly nonlinear systems. We therefore see improvement when implementing a rank based on local dimension over asymptotic dimension, however ~~both~~ all methods produce successful results in this case where all subsystems are sampled in the observations.

We then tested the effectiveness of the reduced rank forecast error covariance matrix in strong CDA when a subsystem is completely unobserved, *i.e.* using only cross-covariances to determine the increment of the unobserved system. The first set of these experiments used observations from the two atmosphere subsystems, extratropical and tropical, while the ocean was left completely unobserved. In this case we found that the DA ~~failed to constrain~~ succeeded in constraining the system to the observations when using the ~~asymptotic dimension~~ full rank, asymptotic dimension, and local dimension to determine the rank of the covariance matrix, however ~~both the variable and full rank methodssucceeded~~the variable-rank method performed better than the fixed-rank methods. The second set of experiments consisted of ENSO observations, or observations from the strongly coupled tropical and ocean subsystems only. In this case, the observational errors and weak coupling to the extratropical subsystem caused the reduced rank experiment to fail. The full rank experiment succeeded in tracking the tropical and ocean subsystems but left the extratropical subsystem unconstrained. This resulted in a collapse of the variance in the ensemble mean and a subsequent reduction in average dimension. However, we found that reducing the observational error variance of the tropical subsystem provided an increase in ensemble mean variance of the extratropical subsystem and therefore an increase in average dimension. Reducing the observational error variance of the ocean did not provide a significant improvement since it is only indirectly coupled to the extratropical subsystem.

The effect of correlated observational errors was also explored. We constructed a trajectory which shadowed the control run and used this as our observational set, repeating all the previous experiments with different observation subsets. Since the correlated errors preserve the underlying dynamical structure of the system, we found that the reduced rank method based on local dimension was ~~more~~ the most successful in all experiments when compared to those using random observational error. This included the ENSO observations case, where the extratropical subsystem remained unconstrained.

Finally, we showed that when only observing the extratropical subsystem, the unobserved subsystems could not be constrained due to their weak or indirect coupling to the observations. This manifested as an overall reduction in dimension as well as a collapse in the cross-domain covariances. In order to counter the covariance and dimension collapse, we introduced a novel scheme for adaptive Kalman gain scaling. This adaptive scaling is based on a measure of the overall spread of the system, therefore accounting for unobserved subsystems that have become unconstrained. Through use of the adaptive scaling the weakly coupled unobserved subsystems were able to be relatively constrained, and moreover the ensemble mean of the unobserved subsystems was able to track the control run. The adaptive scaling introduced here ~~can be applied to general~~ should be tested on additional systems with weak coupling in order to assess its general applicability, although care may need to be taken in the choice of the norm.

We now turn to the implications on more realistic high dimensional systems. It has been shown that when using a finer model resolution (increasing dimension) there is an increase in near-zero asymptotic Lyapunov exponents (De Cruz et al., 2018). We observed through the examination of the dynamical properties of the coupled Lorenz system that the stable yet near-zero exponents have the largest temporal variability which affect the local dimension. As the number of near-zero exponents increase, we may expect that the temporal variability in dimension will increase further. This would have strong implications on the necessary rank of the forecast error covariance and the subsequent number of ensemble members. It is not implausible that the number of ensemble members could vary significantly in time. In such a case where the model degrees of freedom

is much larger than its effective dimension, the projection onto CLVs becomes even more effective. This would ensure the ensemble perturbations lie in subspaces associated with error growth at the given time, and that the directions of error growth are sufficiently sampled. Such improvements in modelling error growth of high dimensional atmospheric systems has already been seen through the use of finite-time normal modes (Wei and Frederiksen, 2005). There is still more work to be done on how CLVs relate to meteorological and climatic events in such models, similar to the blocking studies of Schubert and Lucarini (2016). Future work should also consider the numerical cost of CLV calculation and methods to increase efficiency for high dimensional systems.

The adaptive gain result presented here highlights the utility of ensemble filtering methods. While the ensemble mean of the subsystems manages to track the control run, the individual members are not so constrained. The variability in the spread of the ensemble members can provide a measure for uncertainty of the corresponding subsystem at a given region in phase space. Additionally, the ability to constrain the ensemble mean of the system from only observations of the weakly coupled fast subsystem is a new result for strong CDA. While dynamically this is intuitive (accurate knowledge of the fast dynamics of a system is sufficient to reconstruct the full attractor), this has not previously been shown to be achievable in DA experiments. If such a scheme could be shown to scale to high dimensional climate models, then accurate and frequent atmospheric observations could potentially be sufficient to constrain the full system. For this reason it is important that the scheme be analysed for general applicability and tested on a variety of coupled dynamical systems.

Appendix A: Limiting behaviour of adaptive Kalman gain scaling

We address the implication of the adaptive Kalman gain scaling for the two extreme cases: ensemble collapse ($||(\mathbf{X}^f)(\mathbf{X}^f)^{\mathrm{T}}|| \to 0$) and ensemble ~~blow-up~~ divergence ($||(\mathbf{X}^f)(\mathbf{X}^f)^{\mathrm{T}}|| \to \infty$).

1. $||(\mathbf{X}^f)(\mathbf{X}^f)^{\mathrm{T}}|| \to 0$:

   We consider the Kalman gain in the form

   $$\mathbf{K} = \delta\mathbf{P}^f\mathbf{H}^{\mathrm{T}}[\delta\mathbf{H}\mathbf{P}^f\mathbf{H}^{\mathrm{T}} + \mathbf{R}]^{-1}, \tag{A1}$$

   where $\delta = ||(\mathbf{X}^f)(\mathbf{X}^f)^{\mathrm{T}}||$ and the subscript from equation (9a) has been dropped for brevity. For $\delta \ll 1$, equation (A1) can be expanded to

   $$\begin{aligned}\mathbf{K} &= \delta\mathbf{P}^f\mathbf{H}^{\mathrm{T}}[\mathbf{R}^{-1} - \delta\mathbf{R}^{-1}\mathbf{H}\mathbf{P}^f\mathbf{H}^{\mathrm{T}}\mathbf{R}^{-1} + \mathcal{O}(\delta^2)] \\ &= \delta\mathbf{P}^f\mathbf{H}^{\mathrm{T}}\mathbf{R}^{-1} - \delta^2\mathbf{P}^f\mathbf{H}^{\mathrm{T}}\mathbf{R}^{-1}\mathbf{H}\mathbf{P}^f\mathbf{H}^{\mathrm{T}}\mathbf{R}^{-1} + \mathcal{O}(\delta^3).\end{aligned} \tag{A2}$$

   Letting $\delta \to 0$, equation (A2) simplifies to $\mathbf{K} = \mathbf{0}$, the zero matrix. In this case the mean analysis increment and error covariance equations (9b-9c) simplify to

   $$\overline{\boldsymbol{x}}^a = \overline{\boldsymbol{x}}^f, \tag{A3}$$

   $$\mathbf{P}^a = \mathbf{P}^f. \tag{A4}$$

In other words, in the case of collapsed spread, the analysis is equal to the forecast.

2. $||(\mathbf{X}^f)(\mathbf{X}^f)^{\mathrm{T}}|| \to \infty$:

We consider the Kalman gain in the form

$$\mathbf{K} = \mathbf{P}^f\mathbf{H}^{\mathrm{T}}[\mathbf{H}\mathbf{P}^f\mathbf{H}^{\mathrm{T}} + \delta\mathbf{R}]^{-1}, \tag{A5}$$

where $\delta = \frac{1}{||(\mathbf{X}^f)(\mathbf{X}^f)^{\mathrm{T}}||}$. For $\delta \ll 1$, equation (A5) can be expanded to

$$\mathbf{K} = \mathbf{P}^f\mathbf{H}^{\mathrm{T}}[(\mathbf{H}\mathbf{P}^f\mathbf{H}^{\mathrm{T}})^{-1} - \delta(\mathbf{H}\mathbf{P}^f\mathbf{H}^{\mathrm{T}})^{-1}\mathbf{R}(\mathbf{H}\mathbf{P}^f\mathbf{H}^{\mathrm{T}})^{-1} + \mathcal{O}(\delta^2)]. \tag{A6}$$

Letting $\delta \to 0$, equation (A6) simplifies to

$$\mathbf{K} = \mathbf{P}^f\mathbf{H}^{\mathrm{T}}(\mathbf{H}\mathbf{P}^f\mathbf{H}^{\mathrm{T}})^{-1}. \tag{A7}$$

In this case the mean analysis increment and error covariance equations (9b-9c) become

$$\overline{\boldsymbol{x}}^a = \overline{\boldsymbol{x}}^f + \mathbf{P}^f\mathbf{H}^{\mathrm{T}}(\mathbf{H}\mathbf{P}^f\mathbf{H}^{\mathrm{T}})^{-1}(\boldsymbol{y} - \mathbf{H}\overline{\boldsymbol{x}}^f), \tag{A8}$$

$$\mathbf{P}^a = \big(\mathbf{I} - \mathbf{P}^f\mathbf{H}^{\mathrm{T}}(\mathbf{H}\mathbf{P}^f\mathbf{H}^{\mathrm{T}})^{-1}\mathbf{H}\big)\mathbf{P}^f. \tag{A9}$$

Recall that $\boldsymbol{y}$ are the observations defined by $\boldsymbol{y} = \mathbf{H}\boldsymbol{x}$ where $\boldsymbol{x}$ is the truth (the observation error has implicitly been set as zero in the case of large spread). For a function $\mathcal{F}$ with a Taylor series expansion operating on two arbitrary matrices $\mathbf{A}$ and $\mathbf{B}$, we have the following identity:

$$\mathcal{F}(\mathbf{A}\mathbf{B})\mathbf{A} = \mathbf{A}\mathcal{F}(\mathbf{B}\mathbf{A}) \tag{A10}$$

Taking $\mathbf{A} = \mathbf{H}$, $\mathbf{B} = \mathbf{P}^f\mathbf{H}^{\mathrm{T}}$, and $\mathcal{F}$ the inverse function, we can simplify (A8-A9) to

$$\overline{\boldsymbol{x}}^a = \boldsymbol{x}, \tag{A11}$$

$$\mathbf{P}^a = \mathbf{0}. \tag{A12}$$

In such a case, all ensemble members are adjusted to the same value as inferred from the observations.

Author contributions. All authors designed the study. The schemes for the calculation of Lyapunov exponents and CLVs were adapted and implemented by CQ in both Python and Matlab. The Python codes for the ensemble Kalman filtering methods were produced by VK, with modifications by CQ. All figures were produced by CQ. All authors contributed to the direction of the study, discussion of results, and the writing and approval of the manuscript.

Competing interests. The authors declare that they have no conflicts of interest.

Acknowledgements. The authors would like to thank Dylan Harries, Pavel Sakov, and Paul Sandery for their valuable input throughout the preparation of this manuscript, as well as the two anonymous reviewers for their thorough and insightful comments. The authors were supported by the Australian Commonwealth Scientific and Industrial Research Organisation (CSIRO) Decadal Climate Forecasting Project (https://research.csiro.au/dfp).

References

Abarbanel, H. D., Brown, R., and Kennel, M. B.: Variation of Lyapunov exponents on a strange attractor, Journal of Nonlinear Science, 1, 175–199, 1991.

Anderson, J. L. and Anderson, S. L.: A Monte Carlo implementation of the nonlinear filtering problem to produce ensemble assimilations and forecasts, Monthly Weather Review, 127, 2741–2758, 1999.

Benettin, G., Galgani, L., and Strelcyn, J.-M.: Kolmogorov entropy and numerical experiments, Physical Review A, 14, 2338, 1976.

Bishop, C. H., Etherton, B. J., and Majumdar, S. J.: Adaptive sampling with the ensemble transform Kalman filter. Part I: Theoretical aspects, Monthly weather review, 129, 420–436, 2001.

Bocquet, M. and Carrassi, A.: Four-dimensional ensemble variational data assimilation and the unstable subspace, Tellus A: Dynamic Meteorology and Oceanography, 69, 1304 504, 2017.

Bocquet, M., Raanes, P. N., and Hannart, A.: Expanding the validity of the ensemble Kalman filter without the intrinsic need for inflation, Nonlinear Processes in Geophysics, 22, 645–662, 2015.

Bocquet, M., Gurumoorthy, K. S., Apte, A., Carrassi, A., Grudzien, C., and Jones, C. K.: Degenerate Kalman filter error covariances and their convergence onto the unstable subspace, SIAM/ASA Journal on Uncertainty Quantification, 5, 304–333, 2017.

Bowler, N. E., Flowerdew, J., and Pring, S. R.: Tests of different flavours of EnKF on a simple model, Quarterly Journal of the Royal Meteorological Society, 139, 1505–1519, 2013.

Carrassi, A., Trevisan, A., and Uboldi, F.: Adaptive observations and assimilation in the unstable subspace by breeding on the data-assimilation system, Tellus A: Dynamic Meteorology and Oceanography, 59, 101–113, 2007.

Carrassi, A., Vannitsem, S., Zupanski, D., and Zupanski, M.: The maximum likelihood ensemble filter performances in chaotic systems, Tellus A: Dynamic Meteorology and Oceanography, 61, 587–600, 2008.

Carrassi, A., Bocquet, M., Bertino, L., and Evensen, G.: Data assimilation in the geosciences: An overview of methods, issues, and perspectives, Wiley Interdisciplinary Reviews: Climate Change, 9, e535, 2018.

De Cruz, L., Schubert, S., Demaeyer, J., Lucarini, V., and Vannitsem, S.: Exploring the Lyapunov instability properties of high-dimensional atmospheric and climate models, Nonlinear Processes in Geophysics, 25, 387–412, https://doi.org/10.5194/npg-25-387-2018, https://www.nonlin-processes-geophys.net/25/387/2018/, 2018.

Dieci, L., Russell, R. D., and Van Vleck, E. S.: On the compuation of Lyapunov exponents for continuous dynamical systems, SIAM journal on numerical analysis, 34, 402–423, 1997.

Eckhardt, B. and Yao, D.: Local Lyapunov exponents in chaotic systems, Physica D: Nonlinear Phenomena, 65, 100–108, 1993.

Eckmann, J.-P. and Ruelle, D.: Ergodic theory of chaos and strange attractors, in: The theory of chaotic attractors, pp. 273–312, Springer, 1985.

Evensen, G.: Sequential data assimilation with a nonlinear quasi-geostrophic model using Monte Carlo methods to forecast error statistics, Journal of Geophysical Research: Oceans, 99, 10 143–10 162, 1994.

Evensen, G.: Advanced data assimilation for strongly nonlinear dynamics, Monthly weather review, 125, 1342–1354, 1997.

Evensen, G.: The ensemble Kalman filter: Theoretical formulation and practical implementation, Ocean dynamics, 53, 343–367, 2003.

Frederickson, P., Kaplan, J. L., Yorke, E. D., and Yorke, J. A.: The Liapunov dimension of strange attractors, Journal of differential equations, 49, 185–207, 1983.

Frederiksen, J. S.: Adjoint sensitivity and finite-time normal mode disturbances during blocking, Journal of the atmospheric sciences, 54, 1144–1165, 1997.

Frederiksen, J. S.: Singular vectors, finite-time normal modes, and error growth during blocking, Journal of the atmospheric sciences, 57, 312–333, 2000.

Froyland, G., Hüls, T., Morriss, G. P., and Watson, T. M.: Computing covariant Lyapunov vectors, Oseledets vectors, and dichotomy projectors: A comparative numerical study, Physica D: Nonlinear Phenomena, 247, 18–39, 2013.

Ginelli, F., Poggi, P., Turchi, A., Chaté, H., Livi, R., and Politi, A.: Characterizing dynamics with covariant Lyapunov vectors, Physical review letters, 99, 130 601, 2007.

Gritsun, A. and Lucarini, V.: Fluctuations, response, and resonances in a simple atmospheric model, Physica D: Nonlinear Phenomena, 349, 62–76, 2017.

Grudzien, C., Carrassi, A., and Bocquet, M.: Asymptotic forecast uncertainty and the unstable subspace in the presence of additive model error, SIAM/ASA Journal on Uncertainty Quantification, 6, 1335–1363, 2018a.

Grudzien, C., Carrassi, A., and Bocquet, M.: Chaotic dynamics and the role of covariance inflation for reduced rank Kalman filters with model error, Nonlinear Processes in Geophysics, 25, 633–648, 2018b.

Gurumoorthy, K. S., Grudzien, C., Apte, A., Carrassi, A., and Jones, C. K.: Rank deficiency of Kalman error covariance matrices in linear time-varying system with deterministic evolution, SIAM Journal on Control and Optimization, 55, 741–759, 2017.

Hamill, T. M., Whitaker, J. S., and Snyder, C.: Distance-dependent filtering of background error covariance estimates in an ensemble Kalman filter, Monthly Weather Review, 129, 2776–2790, 2001.

Han, G., Wu, X., Zhang, S., Liu, Z., and Li, W.: Error covariance estimation for coupled data assimilation using a Lorenz atmosphere and a simple pycnocline ocean model, Journal of Climate, 26, 10 218–10 231, 2013.

Houtekamer, P. L. and Zhang, F.: Review of the Ensemble Kalman Filter for Atmospheric Data Assimilation, Monthly Weather Review, 144, 4489–4532, 2016.

Hunt, B. R., Kostelich, E. J., and Szunyogh, I.: Efficient data assimilation for spatiotemporal chaos: A local ensemble transform Kalman filter, Physica D: Nonlinear Phenomena, 230, 112–126, 2007.

Kang, J.-S., Kalnay, E., Liu, J., Fung, I., Miyoshi, T., and Ide, K.: "Variable localization" in an ensemble Kalman filter: Application to the carbon cycle data assimilation, Journal of Geophysical Research: Atmospheres, 116, 2011.

Kaplan, J. L. and Yorke, J. A.: Chaotic behavior of multidimensional difference equations, in: Functional Differential equations and approximation of fixed points, pp. 204–227, Springer, 1979.

Kwasniok, F.: Fluctuations of finite-time Lyapunov exponents in an intermediate-complexity atmospheric model: a multivariate and large-deviation perspective, Nonlinear Processes in Geophysics, 26, 195–209, 2019.

Laloyaux, P., Balmaseda, M., Dee, D., Mogensen, K., and Janssen, P.: A coupled data assimilation system for climate reanalysis, Quarterly Journal of the Royal Meteorological Society, 142, 65–78, 2016.

Lorenz, E. N.: Deterministic nonperiodic flow, Journal of the atmospheric sciences, 20, 130–141, 1963.

Lorenz, E. N.: Predictability: A problem partly solved, in: Proc. Seminar on predictability, vol. 1, 1996.

Miller, R. N., Ghil, M., and Gauthiez, F.: Advanced data assimilation in strongly nonlinear dynamical systems, Journal of the atmospheric sciences, 51, 1037–1056, 1994.

Nese, J. M. and Dutton, J. A.: Quantifying predictability variations in a low-order occan-atmosphere model: a dynamical systems approach, Journal of climate, 6, 185–204, 1993.

Ng, G.-H. C., Mclaughlin, D., Entekhabi, D., and Ahanin, A.: The role of model dynamics in ensemble Kalman filter performance for chaotic systems, Tellus A: Dynamic Meteorology and Oceanography, 63, 958–977, 2011.

Norwood, A., Kalnay, E., Ide, K., Yang, S.-C., and Wolfe, C.: Lyapunov, singular and bred vectors in a multi-scale system: an empirical exploration of vectors related to instabilities, Journal of Physics A: Mathematical and Theoretical, 46, 254 021, 2013.

Oseledets, V. I.: A multiplicative ergodic theorem. Characteristic Ljapunov, exponents of dynamical systems, Trudy Moskovskogo Matematicheskogo Obshchestva, 19, 179–210, 1968.

O'Kane, T. and Frederiksen, J.: Comparison of statistical dynamical, square root and ensemble Kalman filters, Entropy, 10, 684–721, 2008.

O'Kane, T. J., Sandery, P. A., Monselesan, D. P., Sakov, P., Chamberlain, M. A., Matear, R. J., Collier, M. A., Squire, D. T., and Stevens, L.: Coupled Data Assimilation and Ensemble Initialization with Application to Multiyear ENSO Prediction, Journal of Climate, 32, 997–1024, 2019.

Palatella, L. and Trevisan, A.: Interaction of Lyapunov vectors in the formulation of the nonlinear extension of the Kalman filter, Physical Review E, 91, 042 905, 2015.

Palatella, L., Carrassi, A., and Trevisan, A.: Lyapunov vectors and assimilation in the unstable subspace: theory and applications, Journal of Physics A: Mathematical and Theoretical, 46, 254 020, 2013.

Peña, M. and Kalnay, E.: Separating fast and slow modes in coupled chaotic systems, Nonlinear Processes in Geophysics, 11, 319–327, 2004.

Penny, S., Bach, E., Bhargava, K., Chang, C.-C., Da, C., Sun, L., and Yoshida, T.: Strongly coupled data assimilation in multiscale media: experiments using a quasi-geostrophic coupled model, Journal of Advances in Modeling Earth Systems, 2019.

Raanes, P. N., Bocquet, M., and Carrassi, A.: Adaptive covariance inflation in the ensemble Kalman filter by Gaussian scale mixtures, Quarterly Journal of the Royal Meteorological Society, 145, 53–75, 2019.

Sakov, P. and Oke, P. R.: Implications of the form of the ensemble transformation in the ensemble square root filters, Monthly Weather Review, 136, 1042–1053, 2008.

Sakov, P. and Sandery, P.: An adaptive quality control procedure for data assimilation, Tellus A: Dynamic Meteorology and Oceanography, 69, 1318 031, 2017.

Sakov, P., Oliver, D. S., and Bertino, L.: An iterative EnKF for strongly nonlinear systems, Monthly Weather Review, 140, 1988–2004, 2012.

Sano, M. and Sawada, Y.: Measurement of the Lyapunov spectrum from a chaotic time series, Physical review letters, 55, 1082, 1985.

Schubert, S. and Lucarini, V.: Covariant Lyapunov vectors of a quasi-geostrophic baroclinic model: analysis of instabilities and feedbacks, Quarterly Journal of the Royal Meteorological Society, 141, 3040–3055, 2015.

Schubert, S. and Lucarini, V.: Dynamical analysis of blocking events: spatial and temporal fluctuations of covariant Lyapunov vectors, Quarterly Journal of the Royal Meteorological Society, 142, 2143–2158, 2016.

Sluka, T. C., Penny, S. G., Kalnay, E., and Miyoshi, T.: Assimilating atmospheric observations into the ocean using strongly coupled ensemble data assimilation, Geophysical Research Letters, 43, 752–759, 2016.

Tippett, M. K., Anderson, J. L., Bishop, C. H., Hamill, T. M., and Whitaker, J. S.: Ensemble square root filters, Monthly Weather Review, 131, 1485–1490, 2003.

Trevisan, A. and Palatella, L.: On the Kalman Filter error covariance collapse into the unstable subspace, Nonlinear Processes in Geophysics, 18, 243–250, 2011.

Trevisan, A. and Uboldi, F.: Assimilation of standard and targeted observations within the unstable subspace of the observation–analysis–forecast cycle system, Journal of the atmospheric sciences, 61, 103–113, 2004.

Trevisan, A., D'Isidoro, M., and Talagrand, O.: Four-dimensional variational assimilation in the unstable subspace and the optimal subspace dimension, Quarterly Journal of the Royal Meteorological Society: A journal of the atmospheric sciences, applied meteorology and physical oceanography, 136, 487–496, 2010.

Vannitsem, S.: Predictability of large-scale atmospheric motions: Lyapunov exponents and error dynamics, Chaos: An Interdisciplinary Journal of Nonlinear Science, 27, 032 101, 2017.

Vannitsem, S. and Lucarini, V.: Statistical and dynamical properties of covariant Lyapunov vectors in a coupled atmosphere-ocean model—multiscale effects, geometric degeneracy, and error dynamics, Journal of Physics A: Mathematical and Theoretical, 49, 224 001, 2016.

Wei, M. and Frederiksen, J. S.: Finite-time normal mode disturbances and error growth during Southern Hemisphere blocking, Advances in Atmospheric Sciences, 22, 69–89, 2005.

Wolfe, C. L. and Samelson, R. M.: An efficient method for recovering Lyapunov vectors from singular vectors, Tellus A: Dynamic Meteorology and Oceanography, 59, 355–366, 2007.

Yoden, S. and Nomura, M.: Finite-time Lyapunov stability analysis and its application to atmospheric predictability, Journal of the Atmospheric Sciences, 50, 1531–1543, 1993.

Yoshida, T. and Kalnay, E.: Correlation-Cutoff Method for Covariance Localization in Strongly Coupled Data Assimilation, Monthly Weather Review, 146, 2881–2889, 2018.

Young, L.-S.: Dimension, entropy and Lyapunov exponents, Ergodic theory and dynamical systems, 2, 109–124, 1982.